results in Table V agree with the results that were obtained by the ultracentrifugation method. Significant amounts of methadone are bound to the plasma proteins in the therapeutic range. The results confirm previous data (12), but disagree markedly from the results of other investigators (9, 10).

REFERENCES

(1) P. Kissinger, *Anal. Chem.*, **46**, 15R (1974).

(2) K. Bean and G. S. King, "Handbook of Derivatives for Chromatography," Heyden and Sons Ltd., London, England, 1978.

(3) W. Sadee and G. C. M. Beelen, "Drug Level Monitoring," Wiley, New York, N.Y., 1980, p. 28.

(4) E. R. Garrett and K. Seyda, *J. Pharm. Sci.*, **72**, 258 (1983).

(5) J. L. Gfeller, G. Frey, J. M. Huen, and J. P. Thevenin, *J. Chromatogr.*, **172**, 141 (1979).

(6) C. Van Buuren, J. F. Lawrence, U. A. Th. Brinkman, I. L. Honigberg, and R. W. Frei, *Anal. Chem.*, **52**, 700 (1980).

(7) J. F. Lawrence, U. A. Th. Brinkman, and R. W. Frei, *J. Chromatogr.*, **185**, 473 (1979).

(8) J. F. Lawrence, U. A. Th. Brinkman, and R. W. Frei, *ibid.*, **171**, 73 (1979).

(9) J. Judis, *J. Pharm. Sci.*, **66**, 802 (1977).

(10) G. D. Olsen, *Clin. Pharm. Ther.*, **14**, 338 (1973).

(11) M. K. Romach, K. M. Piafsky, J. G. Abel, V. Khouw, and E. M. Sellers, *Clin. Pharm. Ther.*, **29**, 211 (1981).

(12) W. H. Horns, M. Rado, and A. Goldstein, *ibid.*, **17**, 636 (1975).

(13) E. R. Garrett and C. A. Hunt, *J. Pharm. Sci.*, **63**, 1056 (1974).

Physical Chemistry of Freeze-drying: Measurement of Sublimation Rates for Frozen Aqueous Solutions by a Microbalance Technique

M. J. PIKAL ˣ, S. SHAH, D. SENIOR, and J. E. LANG

Received October 14, 1981, from *Eli Lilly and Company, Indianapolis, IN 46285.* Accepted for publication April 30, 1982.

Abstract □ The sublimation rate of frozen solutions was studied as a function of freezing rate, thickness of dried product (l), temperature, residual air pressure, and solute concentration. Data are presented for pure water, aqueous potassium chloride, aqueous povidone, and aqueous dobutamine hydrochloride–mannitol (System I). The resistance of the dried product to water vapor flow ($\hat{R}_p$) was evaluated from the sublimation rate and the sample temperature. The primary experimental technique was based on freeze-drying a cylindrical microsample isothermally, with the sample suspended from one arm of a vacuum microbalance. Methodology to evaluate resistance data from vial freeze-drying experiments is also described. In separate experiments, samples in the form of a thin (15-μm) film were visually observed through a microscope during freeze-drying. Freeze-drying of most samples appeared to occur by water vapor escaping through open channels created by prior sublimation of ice. Contrary to the usual theoretical model, $\hat{R}_p$ is neither independent of temperature nor directly proportional to l. Rather, $\hat{R}_p$ decreases with increasing temperature and the l dependence is normally of the form $\hat{R}_p = (A_0 + A_1 l)/(1 + A_2 l)$, where A_i ($i = 0, 1, 2$) are constants. In several cases, $\hat{R}_p$ is very large near $l = 0$, decreases sharply at $l \simeq 0.1$ cm, and obeys the above equation where $l > 0.2$ cm, a result suggesting an amorphous surface skin which cracks on desorption of water. The temperature dependence of $\hat{R}_p$ suggests that, as the sample temperature approaches the eutectic (or collapse) temperature, hydrodynamic surface flow of adsorbed water is an important flow mechanism.

Keyphrases □ Sublimation rate—measurement for frozen aqueous solutions, microbalance technique, as a function of process variables □ Freeze-drying—methodology of rate measurements for aqueous solutions, influence of process variables, mechanisms of mass transfer in the dried solid □ Dosage forms—freeze-drying of aqueous solutions, effect of process variables on sublimation rate, mechanisms for mass transfer through the dried solid

As sublimation of ice proceeds during freeze-drying, a dried product layer above the ice is produced which acts as a barrier, or resistance, for transport of water vapor. The dried product resistance is generally regarded as the most important factor in determining the drying rate at fixed sample temperature and therefore has a major impact on the process economics. However, published experimental data are confined to food products or biological tissue samples, and the effects of major process or formulation variables on the dried product resistance have not been studied.

This report describes the direct experimental determination of the resistance of the dried product as a function of freezing rate, thickness of dried product, temperature, residual air pressure, and solute concentration. Data are presented for aqueous potassium chloride, aqueous povidone, and aqueous dobutamine hydrochloride–mannitol in a 1.12:1 weight ratio (System I)[1]. Sublimation rate data for pure water are also presented. To aid in the interpretation of the resistance data, the freeze-drying process was also observed microscopically using thin (~15-μm) samples confined between two glass coverslips. Procedures for determining the dried product resistance from vial freeze-drying studies are also described. Comparison of resistance data determined from vial freeze-drying with corresponding data determined by the microbalance procedure confirms that microbalance data are indeed predictive of the dried product resistance encountered in vial freeze-drying.

BACKGROUND

Freeze-drying, or lyophilization, is a process where a solvent (normally water) is removed from a frozen solution by sublimation. Freeze-drying has several advantages over competing processes for production of pharmaceuticals. First, as freeze-drying is a low temperature process, chemical decomposition is minimized. Second, since the solution may be sterile filtered immediately before introduction into a vial and no powder-handling steps are involved in the subsequent processing of a parenteral product, particulate levels may be reduced to a minimum. Due to the high capital equipment costs and typically long processing times, freeze-drying is frequently regarded as an expensive process. However, due to a lack of fundamental understanding of freeze-drying, a given process is often not optimized for the maximum production rate consistent with product quality. Consequently, freeze-drying, in practice, often is much more expensive than necessary.

[1] DOBUTREX, Eli Lilly and Co., Indianapolis, Ind.

0022-3549/83/0600-0635$01.00/0

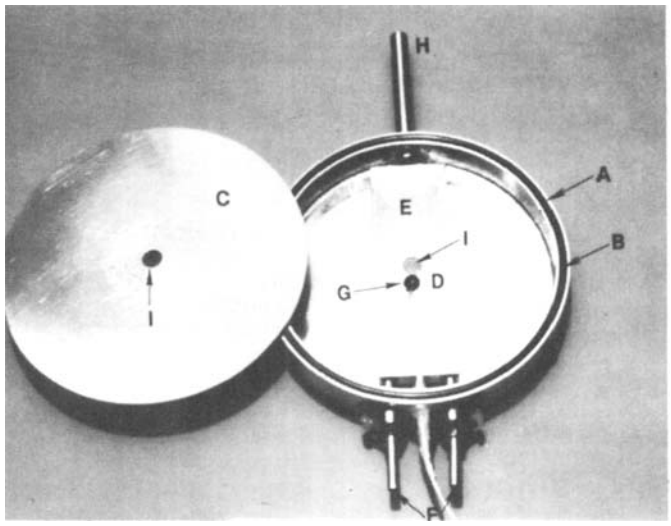

Figure 1—*High-vacuum microscope cold stage. Key: (A) vacuum chamber, (B) rubber seal, (C) lid, (D) sample, (E) temperature-controlled plate, (F) entrance and exit ports (tubes), (G) thermistor surface probe, (H) tube connected to the vacuum line, (I) observation holes.*

The freeze-drying process may be divided into three stages: freezing, primary drying, and secondary drying. For pharmaceutical products, the solution is normally filled into vials to a depth of ~1 cm, and the vials are placed on refrigerated shelves in the freeze-drying chamber. The specific freezing process influences the size and shape of the ice crystals formed and, therefore, affects the structure of the porous solid product remaining after drying (1–3). Thus, the freezing stage may influence strongly the time required to complete the next two steps of the process as well as influence the properties of the final product. After the solutions are frozen the chamber is evacuated, and the shelf temperature is increased to provide energy for the sublimation of ice during primary drying. A frozen solution dries from the top, thereby producing a dried product layer above the ice which increases in thickness as sublimation proceeds. Secondary drying begins locally when all ice has been removed from that region. Thus, in general, secondary drying proceeds simultaneous with primary drying in different regions of the same sample. Normally, secondary drying continues for some time after all ice has been removed from the sample. During secondary drying, the water removed from the solid phase is either bound as a crystalline hydrate or dissolved in an amorphous solid.

The objective of freeze-drying process development is to minimize the process time within the constraints imposed by product quality specifications. Excessive chemical decomposition must be avoided, residual water content often must be low for acceptable stability (4), and the product appearance must conform to standards. To avoid the foaming or puffing that develops during solution vacuum-drying, freeze-drying must be carried out below the eutectic temperature for a crystalline solute or below the collapse temperature for an amorphous solute (2, 3, 5–8). Selection of the shelf temperature and chamber pressure required to maintain the ice temperature just below the eutectic or collapse temperature in all vials during primary drying is a problem in coupled heat and mass transfer. Heat must be transferred from the shelf to the vial bottom and through the frozen solution to the sublimation interface to compensate for the heat removed by sublimation. The rate of heat transfer increases with increased shelf temperature and chamber pressure (9). Therefore, in principle the ice temperature may be maintained constant by adjustment of shelf temperature and chamber pressure.

Assuming that heat is supplied to maintain constant ice temperature, the sublimation rate, and therefore, the total time required for primary drying, will depend on the total resistance to transport of water vapor from the ice–vapor interface to the condenser. The total resistance has three contributors: resistance of the dried product (a porous solid), resistance of the semistoppered vial, and resistance in transfer from the chamber to the condenser. Mass transfer is discussed in terms of resistance, which is defined as the ratio of the difference in water partial pressure to the water flow rate. Resistance is used rather than permeability (the reciprocal of resistance) since the total resistance is additive for component resistances in series. That the dried product resistance is dominant in most freeze-drying applications (10, 11) is supported by theoretical calculations. Using mass flow equations developed for the flow of rarified gases through tubes and orifices (11, 12) and assuming the dried product equivalent to a bundle of capillary tubes, the resistance may be calculated from the dimensions of the vial, stopper, and freeze-dryer and estimates of the pore size of the dried product. Due to the small dimensions of the pores in a typical dried product, flow in the dried product is Knudsen or free molecular flow (11, 12) and contributes ~90% of the total resistance. Clearly, the dried product resistance is an important parameter which may dominate the economics of the freeze-drying process. It is this property with which we are concerned in this study.

The most common procedure used to estimate the dried product resistance is an indirect method which involves measurement of gas flow rate and corresponding pressure difference across a previously freeze-dried specimen of known area and thickness (11). A theoretical model is used to evaluate pore-size parameters for the porous solid which, in turn, are used to calculate the resistance to water vapor flow during ice sublimation from the sample. However, the validity of the model (in particular the assumption that the resistance is directly proportional to the thickness of the dried layer) may be questioned when the dried product is produced from a frozen solution. Microscopic data (2, 3, 13, 14) suggest that the dried product is not necessarily homogeneous, and the mass transfer rate is not always limited by flow in capillary channels. Given the complexity of freeze-drying from frozen solutions, it would seem prudent to avoid the use of theoretical models and evaluate resistances directly from the sublimation rate data.

Quantitative sublimation rate data are available for several frozen systems (15–18), but [with the exception of one study on guinea pig liver (18)] either the vapor pressure difference across the dried product is not available (16–17) or the sample geometry does not allow resistance data to be evaluated for dried product thicknesses of practical interest. A recording high-vacuum microbalance apparatus designed to determine sublimation rates of frozen solutions at controlled temperatures has been described (19). The sample form is a thin (~1-mm) disk of known area. Since the temperature of subliming ice is known and the partial pressure of water at the dried product–vacuum chamber interface is maintained near zero, the water vapor pressure gradient across the dried product is determined and the dried product resistance may be evaluated. The sample holder design limits studies to relatively low sublimation rates (*i.e.*, temperatures <−30°), and the effect of dried product thicknesses characteristic of those encountered in vial freeze-drying (~1 cm) cannot be studied.

The methodology chosen for this research is based on determination of the sublimation rate of a frozen sample with a recording high-vacuum microbalance and, in this respect, is similar to the methodology used by MacKenzie and Luyet (19). However, the sample cell design is more convenient and permits resistance data to be obtained at higher temperatures (~−10°) for dried product thicknesses up to 1 cm. The sample is contained in a 1.3-mm diameter glass tube which is embedded in an aluminum heat exchanger, allowing isothermal operation at the thermostat temperature for most systems of interest.

EXPERIMENTAL

Materials—The potassium chloride used was recrystallized reagent grade material; the mannitol (USP) and povidone (USP, viscosity average molecular weight of 35,000) were used as received. The dobutamine hydrochloride was commercial material[2] used without further purification. Solutions were prepared by weighing the appropriate quantities of distilled water and solute. System I was aqueous dobutamine hydrochloride–mannitol in a 1.12:1 weight ratio with total solids being 53 mg/ml. Conversion of concentration from weight percent to volume percent was accomplished assuming the solute specific volume in solution is the same as that in the solid[3].

Freeze-Drying Microscope—The high-vacuum cold stage (Fig. 1) used in conjunction with an optical microscope[4] for visual observation of freeze-drying is similar to the designs suggested by Flink and Geil-Hansen (20). A nickel-plated brass vacuum chamber (A) ~10 cm in diameter and 1.5 cm in height was sealed using a rubber "O" ring (B) and a stainless steel lid (C). The sample (D) was a thin (~15-μm) film constrained between two glass coverslips. Thermal contact between the bottom coverslip and the temperature-controlled plate (E) was achieved by glueing the coverslip to the plate with silicone stopcock grease. The plate (E) was nickel-plated brass. The distance from the sample to the

[2] Eli Lilly and Co.

[3] Densities used were 1.98 g/ml (potassium chloride), 1.10 g/ml (povidone), and 1.50 g/ml (System I).

[4] Carl Zeiss, Inc.

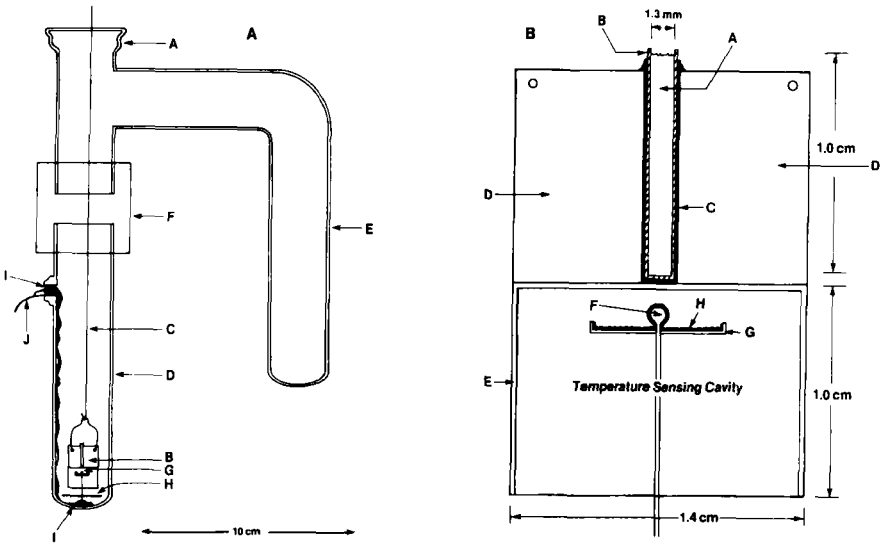

Figure 2—*Microbalance sublimation apparatus. (A) balance tube–condensor assembly, Key: (A) connecting "0" ring joint, (B) sublimation cell (enlarged as Fig. 2B), (C) suspension wire, (D) glass balance tube, (E) glass side arm tube, (F) high-vacuum union, (G) thermocouple probe, (H) heat shield, (I) high-vacuum wax seal, (J) thermocouple wires; (B) sublimation cell, Key: (A) sample, (B) glass capillary tube, (C) high-vacuum wax film, (D and E) top and bottom of the heat exchanger, respectively, (F) thermocouple junction, (G) aluminum disk, (H) thin coat of high-vacuum wax.*

top of the lid was 4–5 mm, allowing the vacuum cold stage to be used with any microscope system having a working distance >5 mm. Temperature control was achieved by passing cold nitrogen gas through channels in the plate. Tubes (F) served as entrance and exit ports for gas flow. The plate was fixed in position ~2 mm from the bottom of the chamber by a plastic spacer (not shown) on the underside of the plate. Temperature of the sample was measured by a thermistor surface probe[5] (G), which was fixed to the top coverslip with silicone stopcock grease. Low pressures (0.02–0.05 torr) were achieved by a tube (H) connected to a vacuum line. Holes (I) cut in the lid and vacuum chamber bottom to allow observation of the sample were covered with glass coverslips sealed to the metal with silicone rubber glue. Rubber supports insulated the cold stage assembly from the microscope stage.

In operation, 5 λ of solution was placed on a 24 × 24-mm coverslip and an 18 × 18-mm coverslip was placed on the droplet, causing the solution to spread evenly over the area of the smaller coverslip. The sample was mounted on the plate (E), the temperature probe (G) was attached, and the lid (C) was placed on the chamber. Nitrogen from a pressurized tank was passed through a 3-Å molecular sieve drying tower and then through copper heat-exchanger coils immersed in liquid nitrogen. Temperature control in the plate was achieved by manual control of the gas flow rate (0–5 liter/min, for ambient to −50°); with periodic adjustment of the nitrogen pressure, temperature control of ±0.5° may be achieved. Accuracy of the temperature measuring system within ±0.5° was established by eutectic and melting point determinations on selected materials spanning the temperature range of interest. The sample was frozen by cooling at a rate of ~1°/min. The samples studied supercooled ~10° below the equilibrium freezing point and froze completely within a few seconds.

Freeze-Drying Microbalance—*Design*—The sample was suspended from one arm of an electronic vacuum microbalance[6] which in turn was connected to a high-vacuum line. For operation at zero pressure, an oil diffusion pump backed by a mechanical pump reduced the air pressure above the sample to ~5×10^{-6} torr. For operation at high residual air pressure, a controlled leak was located ~115 cm downstream from the sample through 2.5-cm diameter tubing. The controlled leak was simply a manually adjusted needle valve. During controlled-leak experiments, only the mechanical pump was operated. Pressure measurements in the range of 0.001–10 torr were made with a capacitance manometer[7] located near the leak site. Residual air pressures <0.001 torr were monitored with a cold cathode ionization gauge[8] ~175 cm downstream from the sample after the vapor stream had passed through a liquid nitrogen cold trap[9].

The sublimation cell, or sample holder, was enclosed by a balance tube–condenser assembly (Fig. 2A) which was connected to the balance using an "0" ring joint (A). The sublimation cell (B) was suspended from the balance beam by a 0.25-mm diameter nichrome wire (C). During operation, the glass balance tube (D) was immersed in a thermostat and the glass side arm tube (E) was immersed in dry ice–acetone to serve as the condenser. A high-vacuum union (F)[10] allowed rapid connection of the balance tube to the rest of the assembly. A copper–constantan thermocouple probe (G) was fitted inside a cylindrical cavity formed by the bottom portion of the sublimation cell. A circular aluminum foil heat shield (H) isolated the thermocouple probe from thermal radiation coming from the sample tube bottom so that the thermocouple probe more accurately sensed the temperature of the sample when the sample and thermostat temperatures differed. High-vacuum wax[11] (I) was used to seal the thermocouple wires (J) to the sample tube (forming a vacuum seal at the point where the wires left the tube) and to support the thermocouple probe in a fixed position at the bottom of the balance tube.

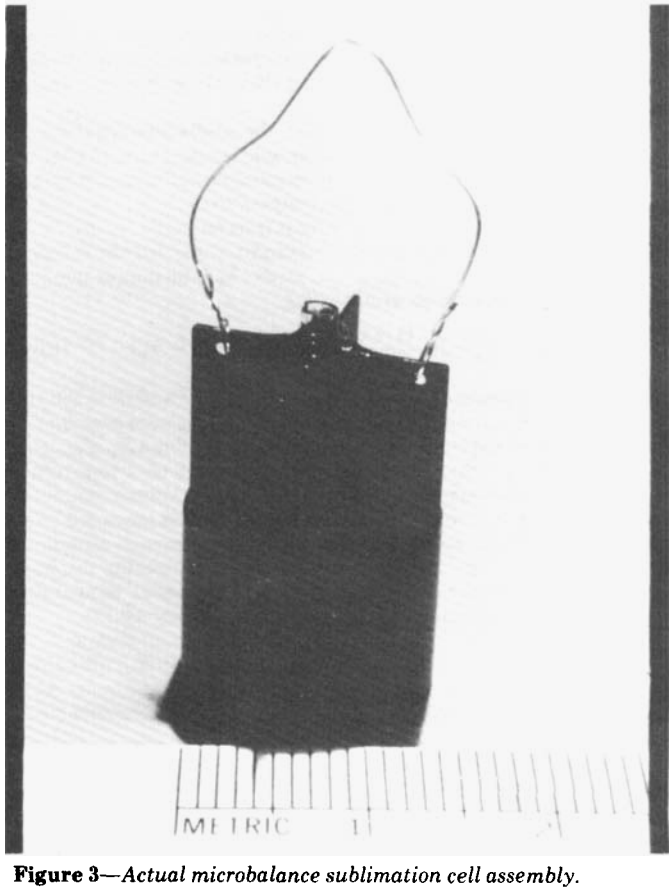

Figure 3—*Actual microbalance sublimation cell assembly.*

[5] Temperature measured with YSI model 42SL telethermometer, Yellow Springs Instrument Co.

[6] Sartorius Model 4102, Brinkmann Instruments, Westbury, NY 11590.

[7] MKS Model 220 Baratron, MKS Instruments, Inc., Burlington, MA 01803.

[8] Kontes/Martin, Evanston, Ill.

[9] Separate experiments indicates that the air pressure measured 175 cm downstream from the sample is a factor of ~5 lower than that above the sample.

[10] CAJON Ultra Torr Union, Cajon Co., Solon, OH 44139.

[11] Apiezon Type W.

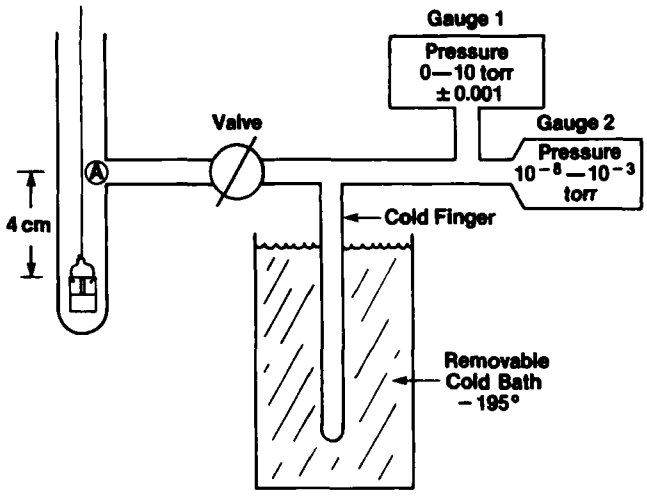

Figure 4—*Balance tube assembly for vapor composition measurements.*

A critical aspect of the sublimation rate measurement is the ability to control and measure the sample temperature. The sublimation cell (Figs. 2B, 3) is essentially a glass capillary tube in good thermal contact with an efficient radiative heat exchanger. This design allows the heat required for sublimation to be transferred from the thermostat to the sample with minimal temperature gradients. The sample (A) was in a glass capillary tube (B) which was fixed into a cylindrical hole in the aluminum heat exchanger by a thin film of high-vacuum wax[11] (C). To maximize radiative heat transfer, the aluminum was given a black anodized finish. The total weight of the sublimation cell was 1.17 g. The top portion of the heat exchanger had four fins (D) at 90° with respect to each other (Fig. 3), while the bottom portion (E) was a cylindrical cavity termed the temperature sensing cavity. The thermocouple probe protruded into this cavity without touching the sublimation cell. To increase the efficiency of heat exchange between the thermocouple probe and the sublimation cell, the effective area of the probe was increased by glueing the thermocouple junction (F) to an aluminum disk (G) with a thin coat of high-vacuum wax (H).

Temperature Measurement—Ideally, the probe measures the cell temperature, which is identical to the sample temperature. In practice, the probe temperature does not exactly measure the cell temperature and, at high sublimation rates, the sample temperature is lower than the cell temperature. A theoretical analysis of heat transfer in the apparatus and a series of calibration experiments (Appendix I) yielded the following relationship between the probe temperature (T_p), the sample temperature (T_s), and ambient temperature (T_a).

$$T_s = T_p - K_p \frac{(1 + 68.1\,P)}{(1 + 87.0\,P)} \dot{m} - K_a(T_a - T_p) \qquad \text{(Eq. 1)}$$

where P is the pressure in the balance tube in torr and $\dot{m}$ is the sublimation rate in mg/min. The parameters K_p and K_a were evaluated by fitting the theoretical model to calibration data, yielding a K_p of 10.2 and K_a of 0.010 at $P = 0$ and K_a of 0.006 for P between 0.05–1 torr, respectively[12]. The probe temperature measured with the system at ambient pressure was identical to the thermostat temperature as measured by the probe thermocouple. Thus, the temperature data for each experiment were corrected for thermocouple inaccuracy by comparing the probe temperature at ambient pressure with the thermostat temperature measured with a glass mercury thermometer (accuracy ±0.1°).

With the above procedures, the magnitude of the uncertainty in T_s was estimated to be 0.5° (due mostly to the uncertainty in K_a) plus 15% of the correction term (Eq. 1) proportional to $\dot{m}$[12]. Thus, the temperature uncertainty was ±0.5° for most of the sublimation experiments but increased to ±1.5° for the experiments with pure water at high temperature and zero pressure.

Background Mass Loss Correction—The rate of mass loss, computed by numerical differentiation from the recorder *versus* time curve[13], contains a background contribution, *i.e.*, mass loss other than sublimation of ice from the sample. The background mass loss arises from loss of adsorbed water from the balance system and the sublimation cell surface; it was determined experimentally by blank runs. No temperature effects were noted between −15 and −25°, and the background effect was assumed to be independent of temperature. The background contribution to the rate of mass loss ($\dot{m}_B$) decreased with time according to the empirical equation:

$$\dot{m}_B = \frac{A}{1 + kt^n} \qquad \text{(Eq. 2)}$$

where t is the time expired after sublimation begins and A, k, and n are constants. With $\dot{m}_B$ in mg/min, the values of A, k, and n, determined by regression analysis of several blank runs, are 0.01252, 0.10836, and 1.0554, respectively. The background correction is significant only for small values of t.

Chamber Pressure and Composition Measurements—Routinely, the pressure in the balance tube and the composition of vapor are not measured. However, such data were determined during representative sublimation experiments. For this series of experiments, a modified balance tube assembly was used (Fig. 4). With the liquid nitrogen cold bath removed, the total pressure at point A was measured using either gauge 1[7] or 2[8], depending on the pressure range studied. The valve was then closed and the cold bath was placed over the cold finger, condensing all water vapor. The residual pressure (due to air) was then measured. This residual pressure was slightly lower than the air pressure in the original vapor since the air remaining in the cold finger was at a lower temperature. The original air pressure was obtained from the measured residual pressure using an empirically determined correction factor (1.10_3 for the apparatus used). The correction factor was determined by measuring the pressure reduction induced by placing the cold bath on the cold finger at high pressure when the vapor was almost entirely air. With the air and total pressures in the sample determined, the water vapor pressure in the sample was obtained by difference[14].

In high-vacuum operation, the mole fraction of water vapor in the sample tube is unity (within experimental error) and the partial pressure of water vapor is <0.01 torr, even for sublimation of pure ice at high temperature. Thus, the partial pressure of water vapor above the sample was negligible compared with the vapor pressure of ice in all experiments carried out at high vacuum. When sublimation was carried out with a controlled air leak into the vacuum system to investigate the effect of air pressure on the sublimation rate, the mole fraction of air in the sample tube (X_2) is found to obey the empirical expression:

$$X_2 = \exp(-0.602\,\dot{m}), \qquad \text{(Eq. 3)}$$

where $\dot{m}$ is the sublimation rate in mg/min. The equation is valid for sublimation from pure ice and frozen solutions over the range in total pressures studied (0.04–0.8 torr). With the frozen solutions studied, $\dot{m}$

[12] Due to a small probe area and significant heat transfer from the ambient through the 30-gauge thermocouple wires (0.023-cm diameter), the thermocouple probe assembly shown here is only partially successful in directly measuring the cell temperature. The design has recently been improved by using smaller thermocouple wire (0.0076-cm diameter) and allowing the wire to equilibrate to the thermostat temperature before entry into the balance tube through the bottom. Also, the probe area is increased by press fitting the thermocouple junction into a finned heat exchanger similar in design to the top portion of the sublimation cell. The area is 1.7 cm², as compared with 0.7 cm² for the probe used to generate the data reported here. With the new finned probe, the value of K_a (Eq. 1) is 0.000 and K_p is 7.1. With the finned probe, the uncertainty in T_s is estimated at ±0.2° with $\dot{m} = 0$.

[13] The balance measures the sum of the gravitational force on the sample and the momentum force resulting from subliming water molecules. As long as the sublimation rate is independent of time, the momentum force is independent of time and the rate of mass loss is correctly computed from the balance readout. However, when the sublimation rate is time dependent, the momentum force is time dependent and contributes to the apparent rate of mass loss (computed from the balance readout). A maximum value for this effect may be estimated by assuming all subliming water molecules leave the sample at right angles to the sample surface. Taking the momentum as the product of the root mean square velocity and the mass of the water molecule, imposing conservation of momentum leads to:

$$\dot{m}_a/\dot{m} = 1 + \frac{1}{g}\left(\frac{3RT}{M_1}\right)^{1/2} \frac{d\ln\dot{m}}{dt}$$

where $\dot{m}_a$ is the apparent (or measured) sublimation rate, $\dot{m}$ is the true sublimation rate, $d\dot{m}/dt$ is the time derivative of the sublimation rate, R is the gas constant, M_1 is the molecular weight of water, T is the absolute temperature, and g is the gravitational constant. Evaluation of the fundamental constants yields:

$$\dot{m}_a/\dot{m} = 1 + 1.0\frac{d\ln\dot{m}}{dt}$$

where time is in min. The correction term $d\ln\dot{m}/dt$ is largest for experiments with pure water at high temperature; but even for this case, the correction is only ~4%.

[14] The cold cathode gauge (gauge 2, Fig. 4) readout was calibrated for air. A calibration curve giving water vapor pressure as a function of gauge reading was obtained by determining the gauge response, while ice in the cold finger slowly sublimed at known temperature and essentially zero air pressure. The water vapor pressure was taken as the equilibrium vapor pressure of ice at the measured temperature corrected for thermal transpiration effects (21).

was small enough that X_2 equaled 1.00 and, even for the studies with pure water, the vapor in the sample tube was mostly air. In experiments with a controlled leak, the total pressure in the balance tube was the same as the total pressure measured at the normal pressure measurement position (located 115 cm downstream from the sample).

Vial Freeze-Drying—*Apparatus*—Vial freeze-drying was carried out in a commercial laboratory freeze-dryer[15] which was modified by inclusion of a temperature-controlled shelf (530 cm^2 area), thermocouple (copper–constantan, 30-gauge) measurement of shelf and product temperature, and pressure measurement[5] in the sample chamber and inside one of the vials.

Pressure inside a vial was measured by connecting a glass tube to the interior of the vial at a location between the vial neck and the top surface of the product. This tube was joined to another tube leading out of the vacuum chamber to the vial pressure sensor. Vial pressure, chamber pressure, and all thermocouple outputs were displayed as a function of time by a 24-channel recorder[16].

Calculation of Sublimation Rate—Calculation of the resistance of the dried product requires the following data: the vapor pressure of ice (evaluated from the product temperature[17]), the pressure in the vial[18], the area of the product (calculated from the vial dimensions), and the sublimation rate. Since the apparatus did not allow the mass of a vial to be monitored continuously, the sublimation rate was evaluated by an alternate procedure.

Phenomenologically the sublimation rate, $\dot{m}$ (in g/hr), is given by:

$$\dot{m} = R_s^{-1}(P_v - P_c) \qquad \text{(Eq. 4)}$$

where R_s is the stopper (or closure) resistance and P_v and P_c are the pressures in the vial and chamber, respectively. Theoretical considerations suggest that the stopper resistance as defined by Eq. 4 should be pressure dependent (12) and may depend slightly on the sublimation rate (22). Empirically for the stoppers used in this research[19], the stopper resistance was found to be essentially independent of sublimation rate and varied with pressure as:

$$R_s = \overline{R}_s/\overline{P} \qquad \text{(Eq. 5)}$$

where $\overline{P}$ is the mean pressure across the stopper [$\overline{P} = (P_v + P_c)/2$)] and, as a first approximation, $\overline{R}_s$ is a constant[20]. Combining Eqs. 4 and 5 yields:

$$\dot{m} = \overline{R}_s^{-1}(P_v^2 - P_c^2)/2 \qquad \text{(Eq. 6)}$$

Since the total mass of water removed during drying (Δm) is known from the solution concentration and fill volume, the value of $\overline{R}_s$ for a given experiment may be evaluated by integration of Eq. 6 over the time period τ_D, where $P_v > P_c$, giving:

$$\overline{R}_s = \frac{1}{2\Delta m}\int_0^{\tau_D}(P_v^2 - P_c^2)dt \qquad \text{(Eq. 7)}$$

where the integration is performed numerically. Since slight variations in stopper placement causes variations in $\overline{R}_s$, a value of $\overline{R}_s$ was determined for each experiment. Once $\overline{R}_s$ was determined using Eq. 7, the sublimation rate at any time during primary drying was evaluated using Eq. 6.

Freezing Procedures—Frozen solutions for microbalance studies were prepared by loading the capillary with 13 λ of solution using a syringe, taking care not to introduce air bubbles. The sublimation cell was suspended from the balance and the balance tube was put into place. The balance tube was then immersed in 2-propanol at −40° (contained in a Dewar flask). When the sample froze, the probe temperature *versus* time plot showed a small change in slope, thereby allowing the freezing temperature to be determined. The studied solutions supercooled 20–25° below the equilibrium freezing point before freezing began. After the probe temperature decreased to <−35°, the 2-propanol bath was removed and the balance tube was immersed in a thermostat at the temperature desired for freeze-drying.

With pure water, 10% v/v potassium chloride, and 22.8% v/v povidone, the temperature history of the sample during freezing was studied by placing two thermocouple junctions (0.0076-cm diameter wire) in the capillary tube. One junction was placed near the tube bottom while the other was placed in the solution at the top of the capillary tube.

NORMALIZED DRIED PRODUCT RESISTANCE

The normalized dried product resistance ($\hat{R}_p$) is defined by:

$$\hat{R}_p = \frac{A_p(P_0 - P_1^D)}{\dot{m}} \qquad \text{(Eq. 8)}$$

where A_p is the geometric cross-sectional area of the product normal to the direction of water vapor flow, P_0 is the equilibrium vapor pressure of ice at the temperature of the subliming ice, P_1^D is the vapor pressure of water above the dried product, and $\dot{m}$ is the sublimation rate. Thus, the normalized dried product resistance is a per-unit-area (or area-normalized) dried product resistance which is a function of the thickness of the dried product layer.

In a vial freeze-drying experiment, P_1^D is the pressure of water vapor in the vial. Since the vapor in the vial during primary drying is essentially all water vapor[18], P_1^D is taken as the measured vial pressure. In a microbalance experiment, P_1^D is essentially zero during high-vacuum operation. During operation with a controlled leak, P_1^D is calculated from the total pressure and the vapor composition given by Eq. 3. Under all conditions studied in this research, P_1^D was small compared to P_0 and was normally negligible. With area in cm^2, pressure in torr, and $\dot{m}$ in g hr^{-1}, the units of $\hat{R}_p$ are cm^2 torr hr g^{-1} and numerically represents the approximate time (in hours) to freeze-dry a solution 1 cm thick at a temperature of −20°.

The thickness of the dried product (l) is evaluated from:

$$l = \frac{m_0 - m_t}{\rho_I A_p \epsilon} \qquad \text{(Eq. 9)}$$

where m_0 is the initial sample mass, m_t is the mass remaining at time t, ρ_I is the density of ice, and ϵ is the porosity or volume fraction of ice. In the microbalance experiment the masses were evaluated directly from the recorder output. In a vial freeze-drying experiment the mass difference, $m_0 - m_t$, was calculated by numerical integration of the sublimation rate over the relevant time interval.

Equation 9 assumes that the ice–vapor boundary remains planar and normal to the axis of the cylindrical container during sublimation. Sublimation of ice from pure ice and frozen aqueous potassium chloride contained in a 1.3-mm diameter capillary tube was examined microscopically by glueing the capillary tube to a glass coverslip and using the aforementioned microscopic observation techniques. The observations demonstrated that this assumption is justified for microbalance experiments. During vial freeze-drying the assumption is valid as a first approximation until near the end of primary drying.

RESULTS AND DISCUSSION

Freezing Rates—Representative data for potassium chloride and povidone are shown in Fig. 5. Onset of freezing is indicated by the sharp increase in temperature, while completion of the freezing process is indicated by a return to the cooling rate characteristic of the sample before

---

[15] Virtis Unitrap.

[16] Esterline Angus Speed Servo II.

[17] Product temperature was routinely measured in the center of the vial at the bottom, in the center about 8 mm up from the bottom, and at the bottom edge. Normally, temperature differences within the vial were small (<1°) and the thermocouple nearest the sublimation surface was used to evaluate the temperature of the subliming ice. If the temperature gradient was significant, the temperature of the ice was calculated using the measured temperature gradient and the estimated distance between the ice interface and the nearest thermocouple.

[18] The partial pressure of water vapor was required but both theoretical calculations and experimental data (23) indicated that the vapor in the vial was essentially 100% water.

[19] In the semistoppered position used during freeze-drying, the 20-mm finish closure has two openings of ~0.4-cm diameter. The 13-mm finish closure, used only for the −15° experiments with System I, has two openings of ~0.2-cm diameter, West Co.

[20] Application of the theories describing flow of rarified gases (12, 22) to the problem of water vapor flow through the closure opening, indicates $\overline{R}_s$ varies with pressure and sublimation rate according to the form:

$$\overline{R}_s^{-1} = a + b\dot{m} + c/[\overline{P}]$$

where a, b and c are constants and the bracket symbols, [ ], indicate the mean for a given experiment. The term in a represents a transport coefficient for viscous flow according to Poiseuille's law, the term in b is a correction of Poiseuille's law for short tubes, and the term in c represents the contribution of free molecular or Knudsen flow. As the pressure decreases and water–stopper collisions become much more frequent than water–water collisions, the term in c dominates and R_s (Eq. 4) becomes independent of pressure.

Regression analysis of $\overline{R}_s$ data for the 20-mm closure determined from Eq. 7 for runs where [P] varied between 0.08 and 0.35 mm and $\dot{m}$ varied between 0.25 and 0.6 g/hr resulted in a = 183, b = −8.0, and c = 3.7. For the pressures and sublimation rates encountered in this research, the term in a dominated, indicating the flow mechanism as mostly viscous. Moreover, during any given experiment designed to measure dried product resistance, variations in $\dot{m}$ and P during primary drying are modest, causing only slight variation in $\overline{R}_s$. Typically, $\overline{R}_s$ deviates from its mean value by no more than ~ ±5% during the portion of primary drying where product resistance data is evaluated, and $\overline{R}_s$ may be regarded as a constant without introducing significant error. For experiments with the 13-mm closure, P was nearly constant so $\overline{R}_s$ also was considered constant.

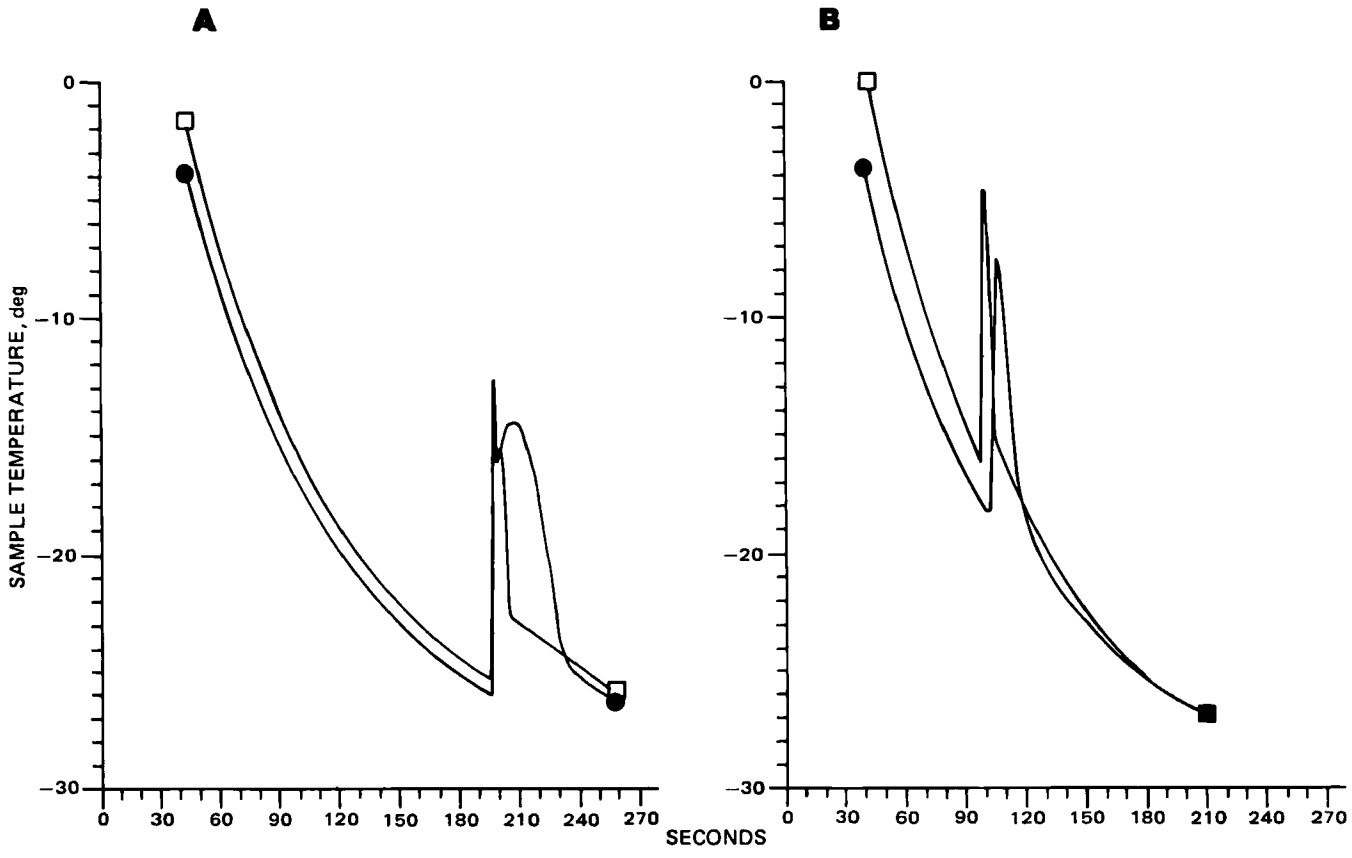

Figure 5—*Freezing curves for microbalance samples of potassium chloride 10% v/v (A) and 22.8% v/v povidone (B). Key: (●) top and (□) bottom of each sample.*

freezing. For both water and potassium chloride, freezing began simultaneously at the top and bottom; for povidone freezing began at the bottom ~4 sec before the top started to freeze. In all cases, freezing was complete at the bottom before the top was completely frozen. The time elapsed between onset and completion of freezing was 13.8 ± 4.2 sec for pure water, 10.2 ± 0.3 sec for povidone, and 31.2 ± 6.0 sec for potassium chloride (mean ± *SD* calculated from replicate experiments).

Cooling curves for the samples frozen in vials qualitatively show the same features exhibited for the microbalance samples (Fig. 5). The samples supercooled, some ice formed throughout the solution quickly, and there was a delay in freezing the remainder of the water, with the top being the last to completely freeze. However, potentially significant quantitative differences exist between the microbalance and vial-freezing behavior. The degree of supercooling for vial-frozen solutions was <50% of that found for the corresponding microbalance solutions, and the time elapsed between onset and completion of freezing was ~30 min for vial-frozen samples. Thus, a vial-frozen sample is subjected to a much slower freezing rate, which may allow ice crystals to anneal or grow in size during freezing.

In both the freeze-drying microscope and microbalance studies, freezing was completed very quickly after the first ice crystals formed; a slow-freezing process which accurately imitates vial freezing was not possible. However, as a first approximation to a vial-freezing process, a sample quick-frozen normally in the microscope or microbalance apparatus was annealed at ~ −8° for 0.5 hr, after which the temperature was reduced to the desired freeze-drying temperature at a rate of ~0.4°/min. This procedure was intended to allow ice crystal growth similar to that which occurs during slow-freezing in a vial.

Microscopic Observation of Freeze-Drying—Photomicrographs (Fig. 6) illustrate the change in structure of a given material on annealing for 0.5 hr at −8°. The darker region at the left of the photograph is the dried sample, while the lighter region on the right still contains ice. Photographs in the left column are quick-frozen samples where the entire sample freezes within seconds, while the right column contains the corresponding annealed samples. Local regions which contain only ice or void are transparent and appear light. The solute is concentrated between the ice crystals and also appears to deposit in a very thin film on the surfaces of the glass coverslips used to contain the sample. The solute concentrated between ice crystals appears dark in both dried and undried regions. The solute deposited on the coverslips is normally semitransparent in the region still containing ice but, at least for crystalline solutes (*i.e.*, potassium chloride), appears dark after the ice has sublimed.

Annealing increased the size of the ice crystals and therefore also increased the size of the voids or pores left after sublimation of the ice. The effect was modest for System I but was marked for both potassium chloride and povidone, where qualitative changes in structure accompanied the growth of ice crystals. The dendrite (1) pattern of ice crystals formed when the aqueous potassium chloride solution froze (Fig. 6A) was lost on annealing (Fig. 6B). The pattern in aqueous povidone (Fig. 6C), which might be classified as irregular dendrite (1, 2), was transformed by annealing to an ice structure largely composed of large globular ice crystals completely surrounded by solute (Fig. 6D). This globular ice structure (Fig. 6C) is qualitatively similar to the ice structure in concentrated (50% solute) aqueous povidone (13).

All nonannealed samples appeared to freeze-dry predominantly by a MacKenzie type I mechanism (13), where water vapor escaped *via* open channels or pores created by prior sublimation of ice until the boundary between dried solute and vacuum chamber (edge of sample) was reached. Both amorphous samples (System I and povidone) showed a glassy region (without ice crystals) at this boundary which developed cracks during drying. This region was presumably a film of solute containing absorbed water which, on partial dehydration, decreased in volume sufficiently to form cracks. Annealed povidone freeze-dried largely by a MacKenzie type II mechanism (13). Here, the water vapor dissolved in and diffused through the solute wall surrounding the ice crystal before leaving the globular cavity. The arrow in the lower center of Fig. 6D indicates the ice–vapor interface in the interior of one partially dried cavity. Thus, the rate of freeze-drying for a type II mechanism potentially is determined by solid-state diffusion of water in the amorphous solute, while the rate for a type I mechanism is determined by flow of water vapor in the porous matrix created by the solute pore structure.

The annealing temperature (−8°) was higher than the eutectic temperature of aqueous potassium chloride (−11°) (24) and the collapse temperature of the povidone used (−17°), but was lower than the collapse temperature of System I[21]. Thus, both potassium chloride and povidone were present in a fluid state during annealing, but the solute in System I was a nonflowable amorphous solid during annealing. The observation that ice crystal growth was rapid in the potassium chloride and povidone

Table I—Microbalance Sublimation Rate Data for Pure Water [a]

n[b]	$t°(l=0)$[c]	$\langle t° \rangle$[d]	P_2^D, torr	A_0	A_1	$\langle \hat{R}_p \rangle$
2	−24	−21.6	0	0.100 ± 0.035[e]	0.175 ± 0.045	0.19 ± 0.02
5	−30	−27.2	0	0.067 ± 0.013	0.153 ± 0.024	0.143 ± 0.005
2	−43	−42.5	0	0.0418 ± 0.0021	0.075 ± 0.003	0.079 ± 0.003
3	−29	−28.4	0.176	0.126 ± 0.038	0.226 ± 0.036	0.24 ± 0.03
2	−29	−28.1	0.309	0.152 ± 0.016	0.313 ± 0.025	0.31 ± 0.02

[a] Parameters for the normalized product resistance equation $\hat{R}_p = A_0 + A_1 l$; units of $\hat{R}_p$ are cm² torr hr g⁻¹. [b] Number of replicate experiments. [c] Temperature of subliming ice at $l = 0$. [d] Mean temperature of subliming ice over the entire experiment. [e] Mean ± *SE*; intended only to provide information on reproducibility between replicate experiments.

systems but slow in System I during annealing suggests that the rate of ice crystal growth is determined, in part, by the fluidity of the solute phase.

Sublimation of Pure Ice—Resistance data calculated from Eq. 8 for pure ice are summarized in Table I. When pure ice is sublimed, $\hat{R}_p$ reflects the resistance in transforming water from the solid state to the vapor state (*i.e.*, the phase change) plus the resistance in transport of water vapor from the ice–vapor interface to the top of the capillary tube. The value of l, as calculated from Eq. 9, is the distance from the ice–vapor interface to the location of this interface at time zero. Since the interface is 0.1 cm below the top of the capillary tube at time zero, the total tube length above the interface (l_T) is given by: $l_T = 0.1 + l$. The $\hat{R}_p$ data were found to increase linearly with increasing l:

$$\hat{R}_p = A_0 + A_1 l \qquad \text{(Eq. 10)}$$

where A_0 and A_1 are constants for a particular temperature. Since the sublimation rates are high and decrease as l increases, the sample temperature increases slightly during an experiment. Thus, both the initial temperature, $t(l = 0)$, and the mean sample temperature during the experiment, $\langle t \rangle$, are reported. The mean normalized product resistance, $\langle \hat{R}_p \rangle$, defined by:

$$\langle \hat{R}_p \rangle = \int_0^1 \hat{R}_p dl \qquad \text{(Eq. 11)}$$

is also tabulated.

The evaporation coefficient (α_v) where $0 < \alpha_v < l$, represents the ratio of the actual sublimation rate to the sublimation rate calculated from simple kinetic theory under conditions of zero resistance offered by the sample container (*i.e.*, the capillary tube). The evaporation coefficient is defined by:

$$\dot{m}(l_T = 0) = \alpha_v A_p \left(\frac{M_1}{2RT}\right)^{1/2} (P_0 - P_1^D) \qquad \text{(Eq. 12)}$$

where $\dot{m}(l_T = 0)$ is the sublimation rate extrapolated to $l_T = 0$, M_1 is the molecular weight of water, R is the gas constant, and T is the absolute temperature (25). All quantities are in CGS units. Combination of Eqs. 8, 10, and 12, evaluation of constants, and conversion to consistent units give:

$$\alpha_v = (1.122)10^{-3}\sqrt{T}/(A_0 - 0.1A_1) \qquad \text{(Eq. 13)}$$

Evaporation coefficients calculated from Eq. 13 and the data in Table I where $P_2^D = 0$ compare favorably with literature data (25–27) (Fig. 7). Since potential errors in sample temperature measurement are much higher for pure ice than for frozen solutions, the agreement shown in Fig. 7 provides strong evidence for the validity of the temperature measurement procedures used in this research.

An increase in residual air pressure (*i.e.*, $P_2^D > 0$) increases both the resistance of the phase change, measured by A_0, and the resistance of the capillary tube, measured by A_1. Both effects presumably originate from collisions between water molecules and air. However, even when P_2^D is approximately equal to the equilibrium vapor pressure of ice (0.350 torr), the sublimation rate remains high, decreasing by a factor of ~2 from the rate at zero pressure.

Dried Product Resistance—*Representation of Data by Empirical Equations*—The variation of normalized product resistance ($\hat{R}_p$) with thickness of dried product (l) is represented by the empirical equation:

$$\hat{R}_p = (A_0 + A_1 l)/(1 + A_2 l), \qquad l' \le l \le 1 \text{ cm} \qquad \text{(Eq. 14)}$$

where $l' = 0$ for most systems studied (*i.e.*, Eq. 14 is valid over the interval $0 \le l \le 1$ cm).

[21] System I does not exhibit a collapse temperature up to −6.5°, where partial melting of the ice crystals (melt-back) occurs.

The parameters A_0, A_1, and A_2 are determined by regression analysis of the raw data. The data are summarized in Table II where the first column provides a curve identification number for each set of experimental conditions, and the corresponding, the A_i ($i = 0, 1, 2$) parameters, mean normalized product resistance ($\langle \hat{R}_p \rangle$), and value of the normalized product resistance at $l = 0$ [$\hat{R}_p(0)$], which are reported in each row. The value of n gives the number of independent replicate experiments. The A_i ($i = 0, 1, 2$) and resistance data tabulated are mean values with the corresponding uncertainty being the standard deviation of the mean. The uncertainty figures are given only to indicate the reproducibility between replicate experiments. Reproducibility of $\hat{R}_p$ data (approximately given by the reproducibility of the corresponding $\langle \hat{R}_p \rangle$ data) was frequently much poorer than one might predict from the scatter in $\hat{R}_p$ *versus* l data from a single experiment, a result perhaps attributable to real differences between samples caused by the inability to precisely control the freezing process. Even for the same chemical system, reproducibility of the raw data (Fig. 8) varies from excellent (curve 16) to poor (curve 15).

In general, Eq. 14 is a valid representation of the raw data even as $l \to 0$, and $\hat{R}_p(0) = A_0$. However, for curves 13, 14, 16, and 17, Eq. 14 is valid only for $l > 0.2$ cm [$\hat{R}_p(0) > A_0$]. In the following discussion all $\hat{R}_p$ *versus* l data were calculated from Eq. 14 where this equation was a valid representation of the raw data. In those cases where Eq. 14 was not valid, mean values of the raw data are used.

Dependence of $\hat{R}_p$ on l—Theoretical models in common use (11, 28) assume the equivalent of $\hat{R}_p \propto l$, which results in the quantity of ice sublimed being directly proportional to the square root of time. Essen-

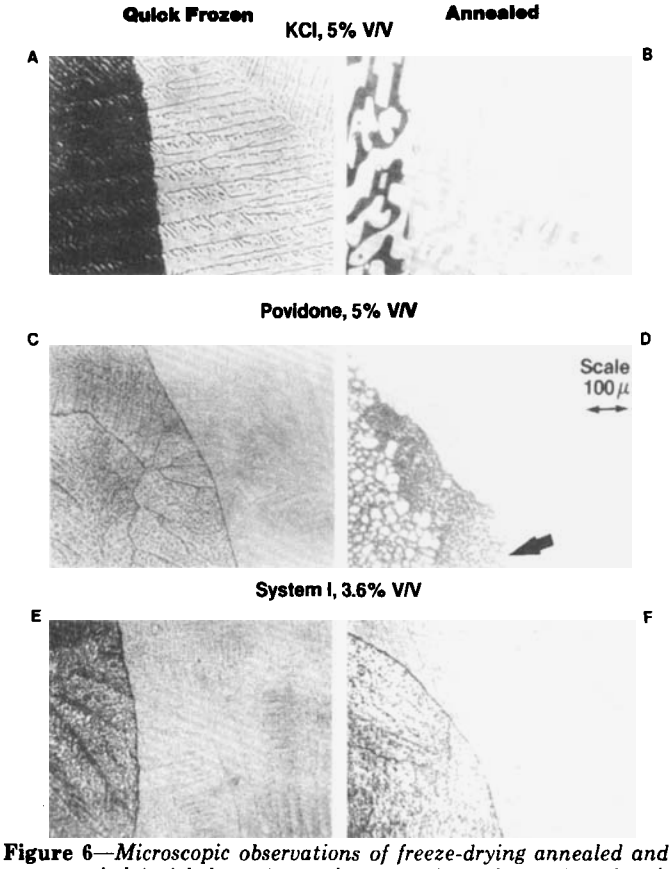

Figure 6—*Microscopic observations of freeze-drying annealed and nonannealed (quick-frozen) samples at −25°. Darker region of each photograph is the dried sample, lighter region still contains ice. The arrow indicates the ice–vapor interface.*

Table II—Microbalance Sublimation Rate Data for Selected Frozen Aqueous Solutions [a]

Curve ID No.	n	Annealed ?	Solute, % (v/v)	$t°$	P_2^Dtorr	A_0	A_1	A_2	$\langle\hat{R}_p\rangle$	$\hat{R}_p(0)$
					Potassium Chloride					
1	2	No	5.0	−13.9	0	1.5 ± 0.6	41.2 ± 4.4	7.7 ± 0.2	4.27 ± 0.16	1.5 ± 0.6
2	6	No	5.0	−20.9	0	2.98 ± 0.29	37.5 ± 4.8	2.90 ± 0.48	8.3 ± 0.6	2.98 ± 0.29
3	2	No	5.0	−29.8	0	2.29 ± 0.25	27.3 ± 0.2	0.93 ± 0.04	10.2 ± 0.1	2.29 ± 0.25
4	4	Yes	5.0	−22.0	0	1.22 ± 0.24	7.1 ± 0.5	0.20 ± 0.08	4.25 ± 0.16	1.22 ± 0.24
5	2	No	5.0	−21.3	0.102	4.7 ± 0.8	30.7 ± 4.7	1.45 ± 0.34	11.0 ± 0.6	4.7 ± 0.8
6	2	No	5.0	−19.6	0.696	3.83 ± 0.37	22.6 ± 3.4	1.57 ± 0.24	8.0 ± 0.1	3.83 ± 0.37
7	2	No	2.5	−21.6	0	1.22 ± 0.18	10.1 ± 1.9	1.05 ± 0.28	3.88 ± 0.07	1.22 ± 0.18
8	2	No	10.0	−19.4	0	0.1 ± 1.7	113 ± 27	4.5 ± 1.3	15.6 ± 0.7	0.1 ± 1.7
					Povidone					
9	3	No	5.0	−26.0	0	1.7 ± 0.3	3.8 ± 1.3	0.00	3.6 ± 0.3	1.7 ± 0.3
10	4	No	5.0	−31.2	0	1.2 ± 0.2	5.2 ± 0.9	0.00	3.8 ± 0.3	1.2 ± 0.3
11	2	Yes	5.0	−26.3	0	0.84 ± 0.16	5.1 ± 1.0	0.50 ± 0.27	2.61 ± 0.06	0.84 ± 0.16
12	2	No	5.0	−31.2	0.186	0.54 ± 0.14	11.5 ± 0.4	0.00	6.3 ± 0.1	0.54 ± 0.14
13	2	No	10.0	−26.2	0	2.9 ± 0.4[b]	3.6 ± 0.2[b]	0.00	4.7 ± 0.5	6.1 ± 0.9[b]
14	2	No	22.8	−25.8	0	3.6 ± 0.6[b]	3.6 ± 0.8[b]	0.00	5.4 ± 0.2	13.3 ± 0.9[b]
					Dobutamine Hydrochloride–Mannitol (System I)					
15	2	No	3.6	−14.0	0	3.3 ± 0.7	50.5 ± 24.3	6.0 ± 3.2	6.8 ± 0.5	3.3 ± 0.7
16	2	No	3.6	−21.2	0	4.0 ± 0.4[b]	24.8 ± 0.6[b]	0.00	18.7 ± 0.1	13.8 ± 1.3
17	2	No	3.6	−21.4	0.190	3.3 ± 1.1[b]	25.6 ± 1.6[b]	0.28 ± .28[b]	16.6 ± 1.4	7.3 ± 4.0

[a] Parameters for the normalized product resistance equation $\hat{R}_p(l) = (A_0 + A_1 l)/(1 + A_2 l)$. [b] Normalized product resistance equation represents data for only $l > 0.2$ cm. As $l \to 0$, the resistance increases to $\hat{R}_p(0)$. Only one of the duplicate experiments on System I at $P_2^D = 0.190$ showed this phenomenon, resulting in the unusually high uncertainty in $\hat{R}_p(0)$.

tially four classes of $\hat{R}_p$ dependence on l have been observed in this research (Fig. 9), none of which correspond to a simple proportionality to l. With the possible exception of curve 8 (Table II), all data show a nonzero intercept at $l = 0$ and the dependence of $\hat{R}_p$ on l is frequently nonlinear. Type I curves show a linear dependence of $\hat{R}_p$ on l throughout the range $0 \leq l \leq 1$. A type II curve exhibits a sharp decrease in $\hat{R}_p$ at low l, followed by a linear increase in $\hat{R}_p$ with increasing l for $l > 0.2$ cm. Type III and type IV curves are concave toward the l axis, the curvature being slight for type III curves but severe for type IV.

The observation that $\hat{R}_p(0)$ is significantly larger than zero suggests the presence of a surface barrier resulting from a different structure for the dried product near the surface, a conclusion consistent with scanning electron microscopic observations (14). A large resistance accompanying the phase change at the ice–vapor interface would give the same result. However, the $\hat{R}_p(0)$ data for solution systems (Table II) are generally one to two orders of magnitude greater than $\hat{R}_p(0)$ for pure ice (Table I), and it does not appear reasonable that the phase change resistance for ice crystallized from a solution would be that much higher than the corresponding resistance for ice crystallized from pure water. As suggested by the microscopic observations discussed earlier, the surface barrier for type II curves appears to be a relatively high-resistance amorphous skin which, after some water desorption, cracks and decreases in effective resistance.

The nonlinearity of the type III and type IV curves may be related, in part, to a gradual variation in dried product structure as l increases. However, the observation that the curvature is temperature dependent (*i.e.*, compare curves 1–3, 15, and 16) indicate that product heterogeneity is not the only factor.

Effect of Solute Concentration on $\hat{R}_p$—An increase in concentration changed the $\hat{R}_p$ *versus* l curve for potassium chloride from a type III to a type IV curve (Fig. 10). The resistance curves for povidone (Fig. 11) show a transition from type I at low concentration to type II at high concentration, where the resistance at $l = 0$ increased sharply at high

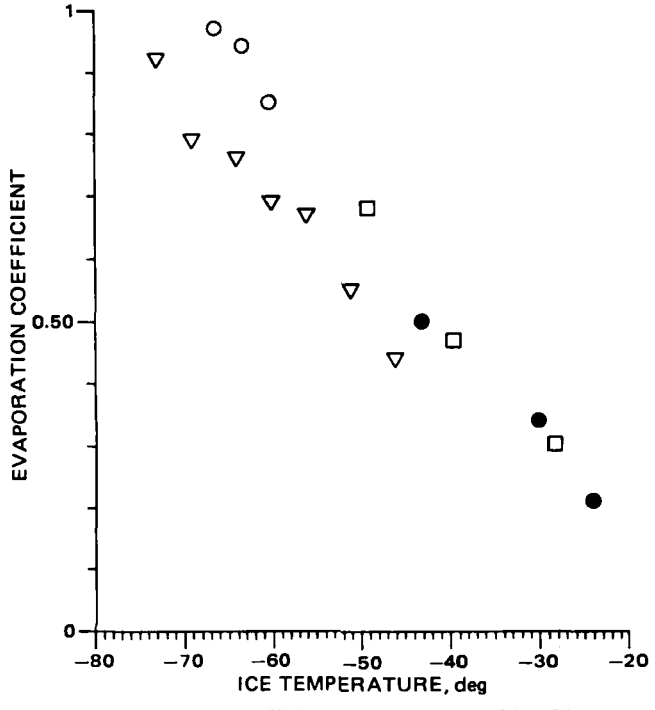

Figure 7—*Evaporation coefficients for ice obtained by this research (●), and (for comparison) taken from Refs. 25 (□), 26 (○), and 27 (▽).*

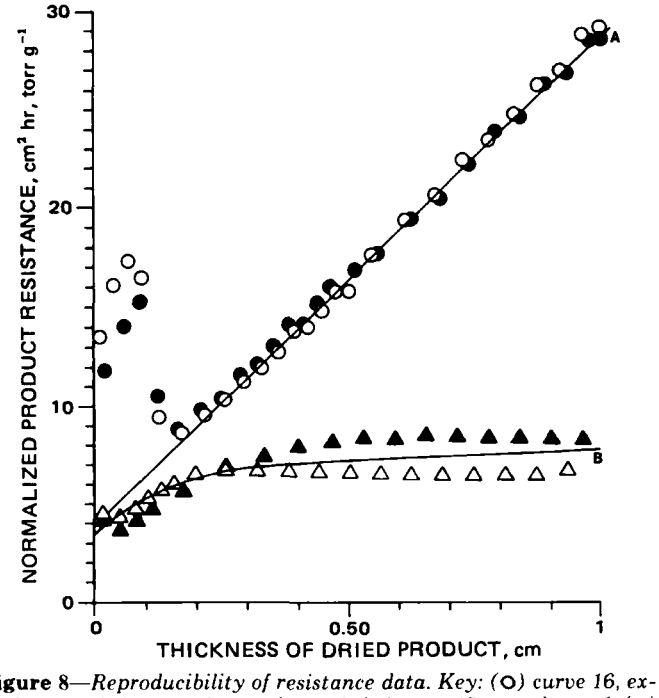

Figure 8—*Reproducibility of resistance data. Key: (○) curve 16, experiment 1; (●) curve 16, experiment 2; (△) curve 15, experiment 1; (▲) curve 15, experiment 2. The lines represent predictions of curves 16 (A) and 15 (B) calculated using Eq. 29.*

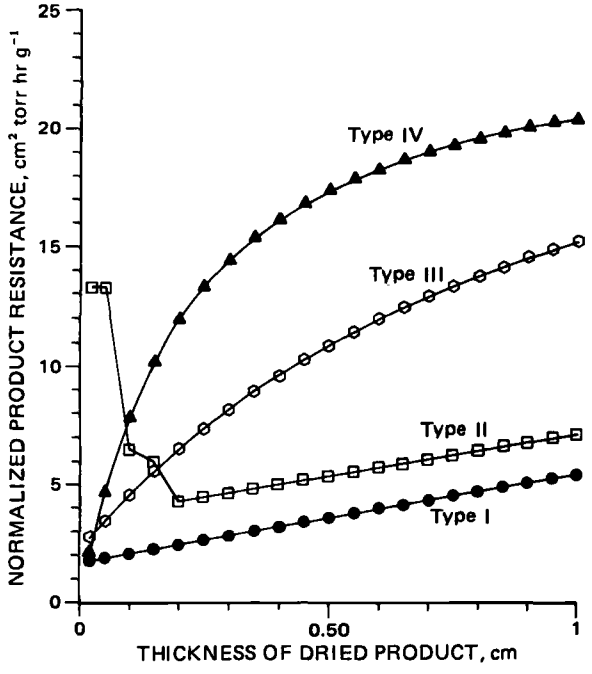

Figure 9—*Curves for $\hat{R}_p$ dependence on dried product thickness. Key: (●) 5% povidone at −26°, type I; (□) 22.8% povidone at −26°, type II; (○) 5% potassium chloride at −30°, type III; (▲) 10% potassium chloride at −20°, type IV.*

concentration. Evidently, the postulated amorphous skin phenomenon increases in significance as the concentration increases.

The mean normalized product resistance ($\langle \hat{R}_p \rangle$) increased as the concentration increased (Fig. 12). For potassium chloride, the increase was essentially linear in volume percent solid, while in the case of povidone, $\langle \hat{R}_p \rangle$ increased sharply with increasing concentration only at low concentration. Above ~10% solute (v/v), $\langle \hat{R}_p \rangle$ for povidone is nearly independent of concentration. Therefore, the drying time for a 1-cm deep potassium chloride solution will be twice as long for a 10% as for a 5% solution[22]. As a first approximation, the drying time for a 1-cm deep povidone solution is independent of concentration between 10% and at least 23% solute.

Effect of Annealing—The microscopic studies (Fig. 6) indicate that annealing resulted in larger ice crystals with correspondingly larger voids or pores in the dried solid. For potassium chloride, both quick-frozen and annealed samples appeared to freeze-dry by a type I mechanism, but annealing a povidone system caused a change from a type I to a type II freeze-drying mechanism. Assuming resistance decreases as pore size increases, one would expect that annealing the potassium chloride system would result in a lower product resistance. Since annealing a povidone system changes the freeze-drying mechanism, the net effect of annealing on the product resistance is not obvious.

Comparison of quick-frozen with annealed samples shows a significant decrease in $\hat{R}_p$ at all l values on annealing. This effect is very pronounced for potassium chloride (Fig. 13) and smaller, though still significant, for povidone (Fig. 14). Annealing potassium chloride resulted in a transition from a type III curve (nonlinear) to a curve which is nearly type I (linear). Intuitively, one would expect variations in product structure with l to be reduced by annealing. Thus, the observed effect of annealing on the resistance curve type appears consistent with the postulate that curvature in a resistance curve is related to structural heterogeneity.

[22] The reviewer suggested that the concentration dependence of $\langle \hat{R}_p \rangle$ for potassium chloride may be related to the increase in the ratio of eutectic–pre-eutectic ice as the solute concentration increases. Eutectic ice refers to ice which crystallizes with simultaneous crystallization of solute while pre-eutectic ice denotes ice formed prior to the crystallization of solute. Assuming equilibrium data (24) may be used to calculate the relative amount of eutectic ice formed in a nonequilibrium freezing process, the fraction of ice crystallizing as eutectic ice varies from 0.21 for 2.5% (v/v) to 0.90 for 10% (v/v) potassium chloride. Thus, at 2.5% potassium chloride, $\langle \hat{R}_p \rangle$ should be dominated by the pore structure created by pre-eutectic ice while at 10% potassium chloride the eutectic ice structure should largely determine the resistance behavior. Microscopic observations indicate that eutectic ice is much more finely divided than pre-eutectic ice, and water vapor originating from sublimation of eutectic ice must pass through a network of relatively small pores. Since theory (11) indicates that resistance to vapor flow through pores increases as the pore size decreases, one would expect a higher $\langle \hat{R}_p \rangle$ at higher solute concentration, as observed.

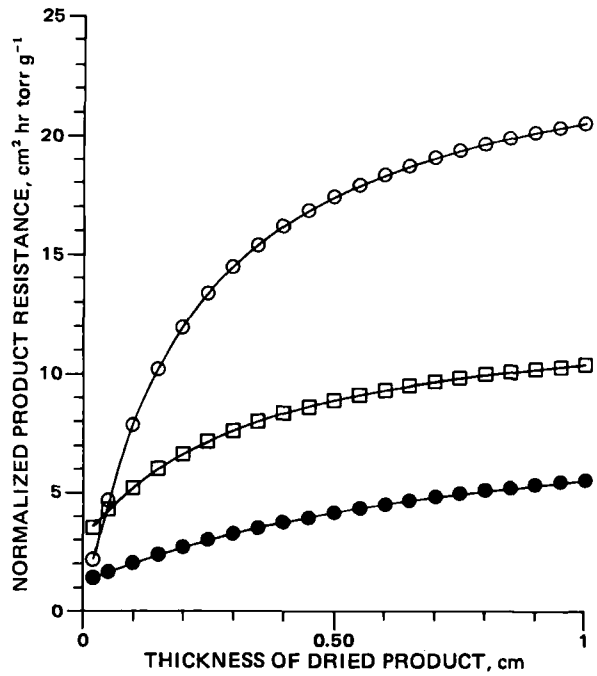

Figure 10—*Effect of solute concentration on $\hat{R}_p$ for potassium chloride at −21°, $P_1^D = 0$. Key: (●) 2.5% v/v; (□) 5.0% v/v; (○) 10.0% v/v.*

Effect of Residual Air Pressure—The data (Table II) indicate a significant increase in $\hat{R}_p$ with increasing air pressure (P_2^D) for 5% povidone at −31° and essentially no pressure effect for System I. The effect of pressure on $\hat{R}_p$ for 5% potassium chloride is small and erratic, probably reflecting sample-to-sample freezing variation more than the effect of pressure. To eliminate the effects of sample variation, the effect of air pressure was studied for a given sample by determining the sublimation rate as a function of pressure at constant l; *i.e.*, during the experiment the pressure was increased stepwise and then decreased stepwise. The mean of the $\hat{R}_p$ values (at corresponding pressures) for the increasing and decreasing parts of the experiment generate a set of $\hat{R}_p$ values at constant l as a function of air pressure. The results (Fig. 15) indicate $\hat{R}_p$ increased with increasing air pressure, the effect being very small for 5% potassium chloride at −21°, but quite significant for 5% povidone at −31°.

One would expect that increasing air pressure would yield an increasing probability of gas phase molecular collisions between water and air. When the frequency of water vapor–air collisions in the dried product becomes comparable in magnitude to the frequency of water vapor collisions with

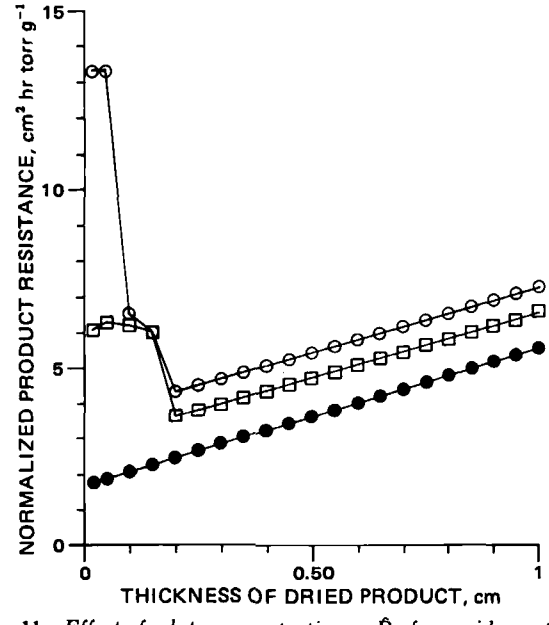

Figure 11—*Effect of solute concentration on $\hat{R}_p$ for povidone at −26°, $P_1^D = 0$. Key: (●) 5.0% v/v; (□) 10.0% v/v; (○) 22.8% v/v.*

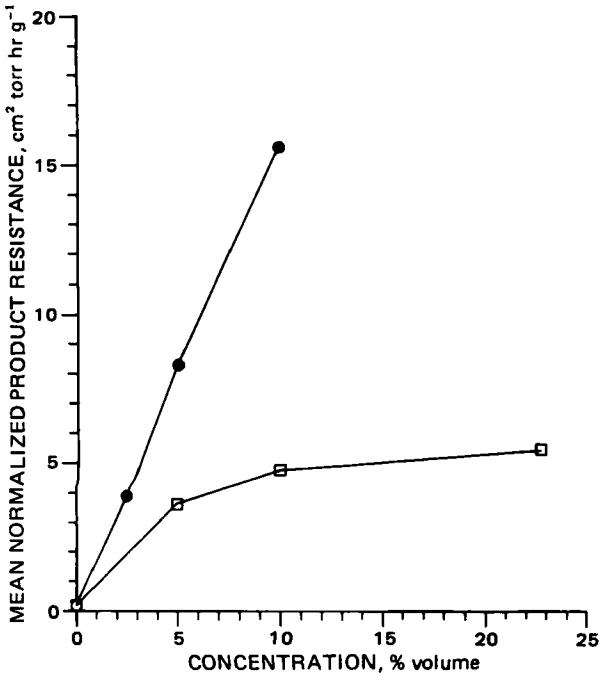

Figure 12—*Mean normalized product resistance ($\langle \hat{R}_p \rangle$) versus solute concentration for (●) potassium chloride at −21°; (□) povidone at −26°.*

the dried product matrix, the resistance due to water–air collisions should become a measurable fraction of the resistance originating from water–matrix collisions. Thus, increasing the air pressure above the sample should increase the product resistance, as observed. As the pore size decreases, the frequency of water–matrix collisions increases and the air pressure at which water–air collisions become comparable to water–matrix collisions will increase. Thus, the product resistance should be less sensitive to air pressure as the pore size decreases. The product resistance of potassium chloride at zero air pressure was much greater than the corresponding resistance for povidone, suggesting that the pore size in freeze-dried potassium chloride is much smaller. Consequently, the slope of the resistance *versus* air pressure curve should be less for potassium chloride than for povidone. The difference in pore size between potassium chloride and povidone is probably a result of the formation

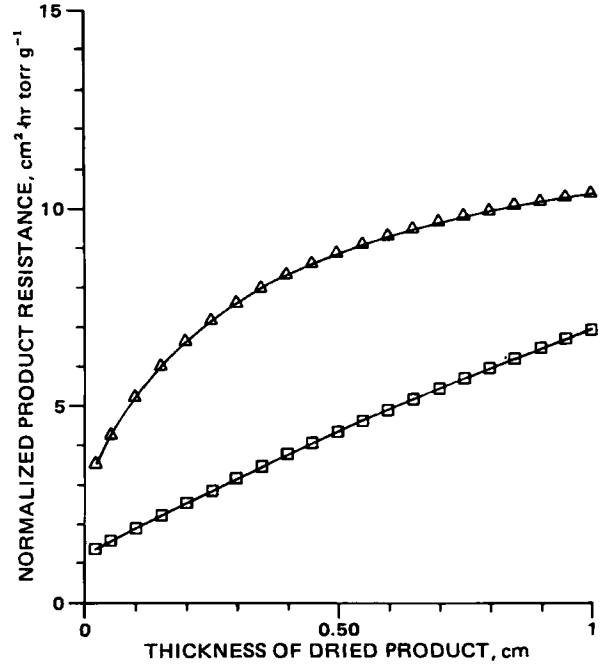

Figure 13—*Effect of annealing on $\hat{R}_p$ for potassium chloride 5% v/v at −21°, P_1^D = 0. Key: (△) not annealed; (□) annealed.*

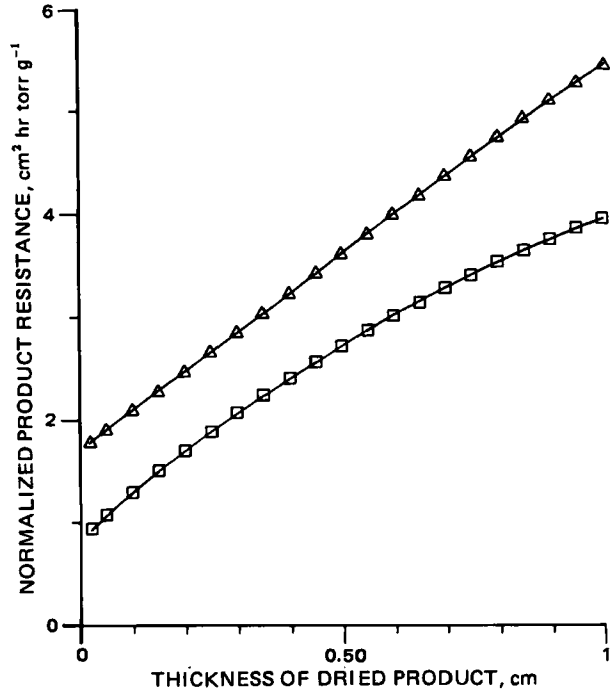

Figure 14—*Effect of annealing on $\hat{R}_p$ for 5% v/v povidone at −26°, P_1^D = 0. Key: (△) not annealed; (□) annealed.*

of eutectic ice in the potassium chloride system. Being amorphous, povidone does not form a eutectic.

The arrows in Fig. 15 indicate the values of the vapor pressure of ice at the corresponding product temperatures (−21.2° for potassium chloride and −31° for povidone). The normalized product resistance increased smoothly as the residual air pressure approached and exceeded the vapor pressure of ice. Thus, the common observation that the sublimation rate decreases sharply as the chamber pressure approaches the vapor pressure of ice (29) is not a result of increasing product resistance. Indeed, sublimation proceeded rapidly even when the residual air pressure was well above the vapor pressure of ice. This apparent anomaly may be resolved by reference to Eq. 8, where the driving force for sublimation is taken as the difference in pressure of water vapor between the ice–vapor

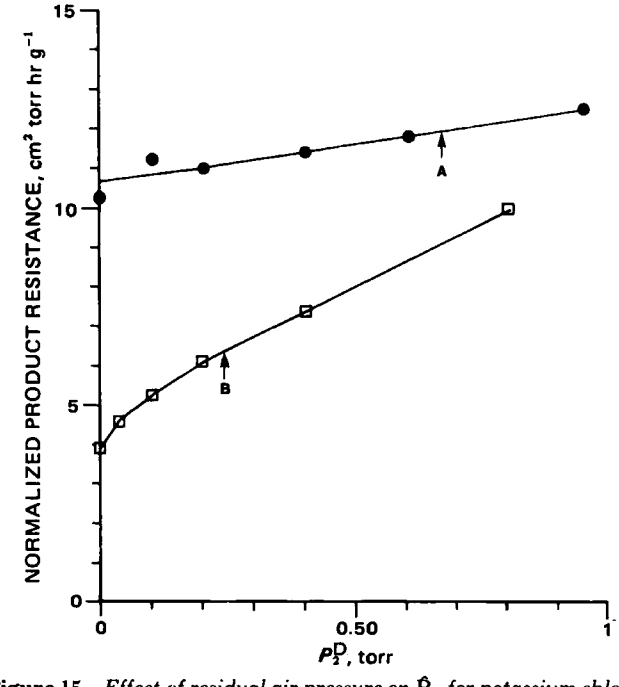

Figure 15—*Effect of residual air pressure on $\hat{R}_p$ for potassium chloride 5% v/v at −21.2°, l = 0.52 cm (●) and 5% v/v povidone at −31.0°, l = 0.70 cm (□). The arrows indicate the vapor pressure of ice (P_0) at −21.2° (A) and −31.0° (B).*

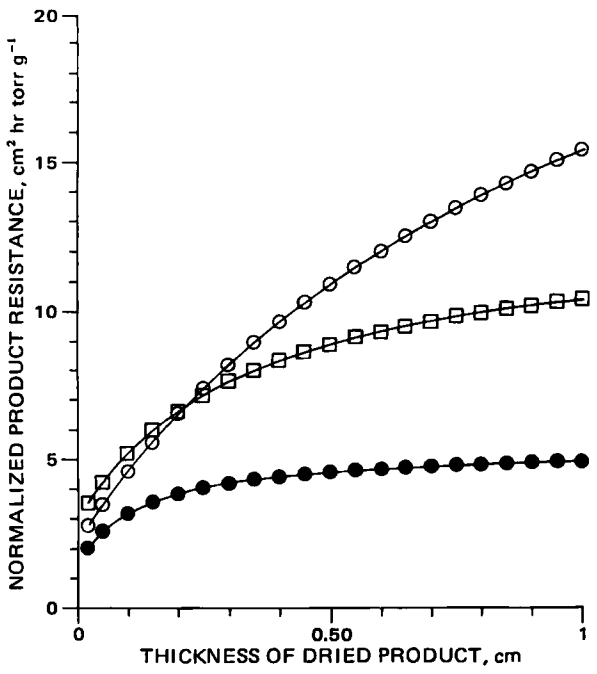

Figure 16—*Effect of temperature on* $\hat{R}_p$ *for potassium chloride 5% v/v,* $P_1^D = 0$. *Key: (●) −13.9°; (□) −20.9°; (○) −29.8°.*

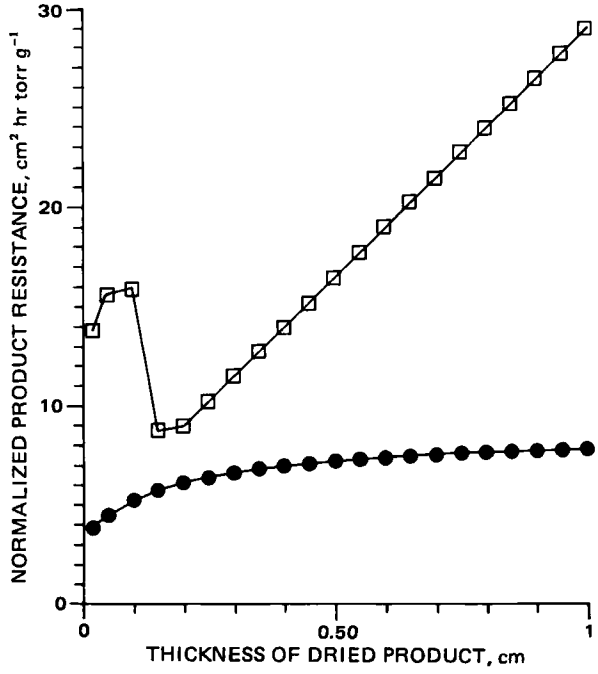

Figure 17—*Effect of temperature on* $\hat{R}_p$ *for System I,* $P_1^D = 0$. *Key: (●) −14.0°; (□) −21.2°.*

interface (P_0) and the region above the dried product (P_1^D). With the microbalance apparatus, P_1^D is essentially zero even when the chamber pressure is well above the vapor pressure of ice. However, in an apparatus designed for vial freeze-drying, an increase in chamber pressure by means of a controlled air leak increases the value of P_1^D. Indeed, as a first approximation, P_1^D is equal to the chamber pressure. If the shelf temperature is adjusted to maintain constant product temperature, P_0 is constant, and the driving force for sublimation decreases sharply as the chamber pressure approaches P_0, thereby sharply decreasing the sublimation rate.

Effect of Temperature—The effect of temperature (Figs. 16–18) on $\hat{R}_p$ is quite dramatic for potassium chloride and System I, but is barely significant for povidone (between −26 and −31°). An increase in temperature resulted in a transition from a type III (potassium chloride) or a type II (System I) curve to a type IV curve with a significant reduction in $(\hat{R}_p)$ (Fig. 19).

It might be postulated that the observed temperature effect is really a pressure effect. That is, the higher temperature produces a higher mean pressure in the porous medium which, in turn, changes the gas flow mechanism from a free molecular (Knudsen) flow to a viscous flow mechanism. For viscous flow, the dried product resistance is inversely proportional to the mean pressure in the dried product (11, 12), which is one-half the vapor pressure of ice for the data in Figs. 16–18. Thus, if the mean pressure were high enough to result in viscous flow of water vapor, an increase in temperature would decrease the dried product resistance. However, based on the usual theories for flow of rarified gases in channels (11, 12), the mean pressure was far too low for viscous flow of water vapor in the dried product.

For the usual capillary-tube model describing gas flow in a porous system (11, 12, 30), the normalized product resistance is given by:

$$\hat{R}_p = \hat{R}_k[1 - (1 - 35\pi/128)X/(1 + X) + (3\pi/128)X^2/(1 + X)]^{-1} \quad \text{(Eq. 15)}$$

where X is the ratio of the capillary pore diameter (D) to the mean free path (λ): $X = D/\lambda$. The low pressure limit for $\hat{R}_p$ is the Knudsen flow resistance ($\hat{R}_k$) which, in CGS units of dynes sec g^{-1}, is given by:

$$\hat{R}_k = l\frac{\tau^2}{\epsilon}\frac{3}{2}\sqrt{\frac{\pi RT}{2M_1}}\frac{(f)}{(2-f)}\frac{1}{D} \quad \text{(Eq. 16)}$$

where τ is the tortuosity (or ratio of the actual length of a capillary tube to the thickness of the dried product) and f denotes a momentum accommodation coefficient representing the fraction of gas molecule–tube collisions which result in diffuse reflectance upon collision (*i.e.*, for diffuse reflectance the velocity of a molecule after collision is independent of its incident velocity). Normally, f is assumed to be unity.

Since the mean free path is inversely proportional to pressure, X approaches zero at low pressure and $\hat{R}_p \to \hat{R}_k$. At high pressure, $X \gg 1$ and transport of water vapor is by a viscous flow mechanism yielding $\hat{R}_p = \hat{R}_k(128/3\pi)/X$. For a freeze-drying experiment where the mean pressure in the dried product is one-half of the vapor pressure of ice, numerical evaluation yields $X = P_0D$ (μm)/146. Thus, the condition $X \gg 1$ implies $D \gg 100$ μm for the highest pressure studied in this research. However, the pore diameters determined either from the sample surface area[23] (30) or microscopic examination (Fig. 6) are $\ll 100$ μm, indicating $X \ll 1$. Thus, the vapor flow mechanism in freeze-drying closely approximates Knudsen flow, not viscous flow.

The pore diameter for freeze-dried potassium chloride evaluated from the surface area is ~10 μm, while the microscopic data (Fig. 6) indicate that the larger pores or channels have a diameter of ~30 μm. Assuming that f is independent of temperature and vapor pressure, and taking D = 30 μm, the calculated change in $\hat{R}_p$ on increasing the temperature from −30 to −14° is an increase of 5%, obviously not consistent with the data which show a decrease in resistance of ~60%.

If the momentum accommodation coefficient (f) were assumed to decrease as the freeze-drying temperature increases, the data could be reconciled with Eqs. 15 and 16. Accommodation coefficients are extremely sensitive to the nature of the surface and, particularly for very clean solid surfaces, may be much less than unity (12, 21, 31). However, as surface impurities are introduced or the vapor is adsorbed on the surface, accommodation coefficients generally increase, and at a surface coverage of one or more monolayers, diffuse scattering (*i.e.*, $f = 1$) is observed (31). This result is consistent with the observation that the energy accommodation coefficient is unity for liquids and their own vapors (31) and the conclusion that under conditions where the energy accommodation coefficient is unity, the momentum accommodation coefficient is also unity (32). Thus, if the surface coverage would decrease below monolayer coverage as the freeze-drying temperature increased, there would be justification for assuming the temperature dependence of $\hat{R}_p$ is due to a decrease in f.

As the temperature increases at constant water activity, the surface coverage will decrease slightly (33), at least in the submonolayer region. However, in the freeze-drying system, an increase in temperature also increases the thermodynamic activity of water, which increases the surface coverage. The net effect of increasing the temperature will depend on the nature of the adsorption isotherm. Extrapolation of adsorption data for water–alkali halide systems (34–36) to the temperature range of interest in freeze-drying indicates that the mean surface coverage in the dried product at −30° is considerably in excess of monolayer, and the

[23] The specific surface areas for vial freeze-dried samples, determined by BET (Brunauer-Emmett-Teller) treatment of gas adsorption, are: potassium chloride (4 m^2/g), povidone (0.7 m^2/g), and System I (3 m^2/g).

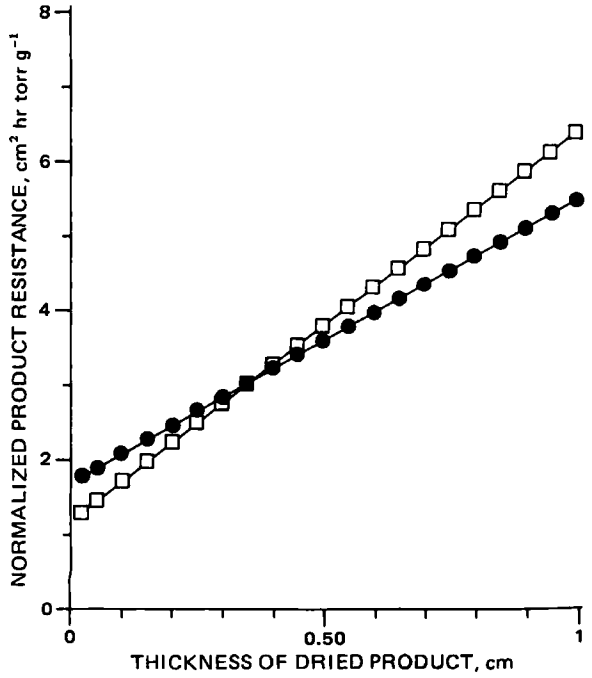

Figure 18—*Effect of temperature on* $\hat{R}_p$ *for 5% v/v povidone,* $P_1^p = 0$. *Key: (●) −26.0; (□) −31.2°.*

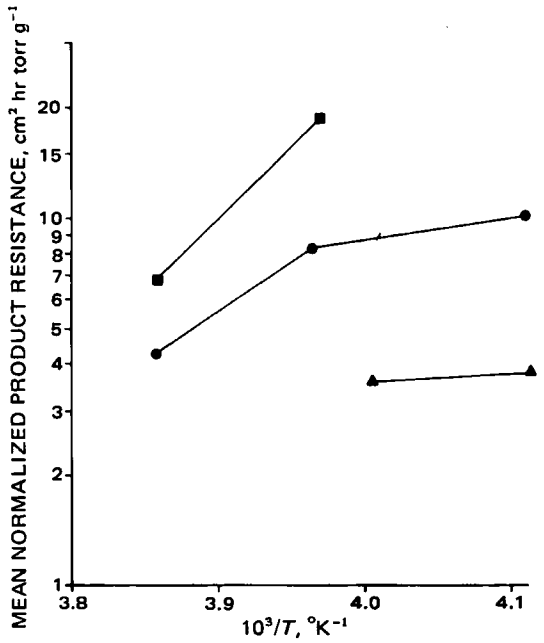

Figure 19—*Mean normalized product resistance* ($\langle \hat{R}_p \rangle$) *versus reciprocal absolute temperature. Key: (▲) povidone, 5% v/v; (●) potassium chloride 5% v/v; (■) System I.*

surface coverage increases with increasing temperature. Thus, the mean momentum accommodation coefficient should be close to unity at all temperatures; if there is a small change in f with increasing temperature, this change should be an increase toward a limiting value of unity. Thus, the observed decrease in resistance as the freeze-drying temperature increases cannot be attributed to changes in f. Rather it appears that there exists some flow mechanism other than that described by Eq. 16.

Equation 16 describes only the flow of water vapor in the open channels of the porous system. However, experimental and theoretical studies of the flow of condensable gases in porous media indicate that surface flow of the adsorbed gas can be the dominant flow mechanism when the mass of the adsorbed phase in the sample greatly exceeds the mass of the vapor phase (30, 37–39). Since the mass of the adsorbed phase is proportional to the product of the specific surface area (S) and the fraction of surface coverage (θ), surface flow may be important even below monolayer coverage (*i.e.*, $\theta < 1$) provided the specific surface area is large. Alternately, surface flow may be important with samples of moderate surface area provided the pressure is high enough to result in multilayer coverage (*i.e.*, $\theta > 1$). In the submonolayer case, surface flow proceeds by a diffusion mechanism involving activated translational motion from an occupied adsorption site to an unoccupied site. In the multilayer case, particularly when $\theta \gg 1$, surface flow is more properly described as hydrodynamic flow of the adsorbed gas analogous to either flow of a thin liquid film along a surface (large pores) or capillary flow of a liquid (micropores).

We therefore postulate that, at least at high temperature where surface coverage is high, mass transfer in freeze-drying may be dominated by hydrodynamic surface flow of the adsorbed water. As the freeze-drying temperature increases, the surface coverage (θ) and the fluidity of the adsorbed phase increase, both effects increasing the rate of surface flow. Adsorption data (34, 40) for potassium chloride indicate that θ increased very rapidly as the thermodynamic activity of water approached the water activity of the saturated solution, and the adsorbed film reached a thickness of 0.1–1 μm before the solid dissolved. Similarly one would expect that, as the temperature of a freeze-drying system approaches the eutectic temperature (or collapse temperature for an amorphous solute), θ would increase rapidly. Indeed, microscopic observations of a potassium chloride–water system freeze-drying near the eutectic temperature (13) of −11° appear consistent with an adsorbed film of liquid ~1 μm in thickness near −13° which decreased sharply in thickness as the temperature decreased. Since the evidence suggests that θ increases dramatically as the eutectic temperature is approached, one might also expect the ratio of surface flow–gas flow to increase as the temperature increases, resulting in surface flow being dominant near the eutectic (or collapse) temperature where θ is very large. Thus, we propose that the observed decrease in dried product resistance resulting from an increase in temperature is a consequence of the emergence of surface flow as an additional flow mechanism for transport of water.

Comparison of Microbalance and Vial Results—The question of how closely a microsample freeze-drying in a capillary tube represents a macrosample freeze-drying in a vial remains. In principle, since the diameter of the capillary tube is much greater than the pore diameter of the dried product, the normalized resistance should be independent of the sample geometry. However, differences in pore structure caused by differences in thermal history are potentially quite important. Moreover, the effect of a nonzero partial pressure of water vapor above the surface of the dried product (0.1 torr for vial studies *versus* 0.00 torr for microbalance studies) may be significant, at least for an amorphous product where the resistance is determined partially by permeability and cracking of the amorphous skin covering the surface.

Since the thermal history of an annealed microbalance sample more closely resembles the thermal history of a vial-frozen sample, one expects better agreement of the vial data with the annealed microbalance samples than with the quick-frozen microbalance samples. Indeed, for potassium chloride the agreement between vial and annealed microbalance results is nearly quantitative (Table III), whereas the quick-frozen microbalance resistance data are higher by nearly a factor of 2. The data for System I (Table III) demonstrate that the effect of temperature is qualitatively the same for both vial- and quick-frozen microbalance results. In both cases, the resistance increased linearly with l for the −21° data, but when the temperature was increased to ~ −15°, the resistance became independent of l over the range of l values studied and the value of $\langle \hat{R}_p \rangle$ decreased. In the case of povidone, the vial resistance data are in much better agreement with the *quick-frozen* microbalance data. This observation may suggest that annealing is a poor approximation for a slow-freeze when the product changes its freeze-drying mechanism on annealing, as is the case with povidone (Fig. 6). In any case, it may be concluded that agreement between vial and microbalance data is at least qualitative and may be quantitative for some materials if the thermal histories of the samples are similar.

CONCLUSIONS

The effect of the potential process variables on the resistance of the dried product layer have been studied by direct determination of sublimation rate under isothermal conditions using a microbalance technique. The results have at least qualitative validity for vial freeze-drying. Contrary to popular theoretical models, the resistance of the dried product layer is not directly proportional to its thickness (a result attributed to heterogeneity in solute structure) and is not independent of temperature. Current theoretical models assume mass transfer is exclusively *via* the gas phase. This study suggests that, at least at higher

temperatures, hydrodynamic surface flow of adsorbed water is an important flow mechanism which may account for the observed temperature dependence of the dried product resistance.

APPENDIX I: HEAT TRANSFER THEORY AND TEMPERATURE MEASUREMENTS

Although the sublimation cell is designed to maximize heat transfer, numerical estimates suggest that, at least for the high sublimation rates expected for pure water, the temperature difference between thermostat and the subliming ice could be significant. In this section, a theoretical model is developed which, on experimental evaluation of heat transfer parameters, allows the ice temperature to be determined from measurement of probe (or thermostat) temperature, sublimation rate, and residual air pressure in the chamber. The heat transfer coefficients were evaluated with a series of sublimation experiments where the sample temperature was measured by a thermocouple (denoted J) embedded in the sample 1 mm from the bottom of the capillary tube.

Assuming steady state:

$$\dot{m}\Delta\overline{H}_s = \dot{Q}_s = \dot{q}_{bc} + \dot{q}_{pc} + \dot{q}_{aJ} + \dot{q}_{ac} \qquad \text{(Eq. A17)}$$

where $\dot{m}$ is the sublimation rate (g/sec), $\Delta\overline{H}_s$ is the heat of sublimation (cal/g), $\dot{Q}_s$ is the rate of heat removal by sublimation, $\dot{q}_{bc}$ is the heat transfer rate from thermostat (bath) to the sublimation cell by radiation and conduction, $\dot{q}_{pc}$ is the heat transfer rate from the probe to the cell by radiation and conduction, $\dot{q}_{aJ}$ is the heat transfer rate from ambient to the J thermocouple junction in the sample through the 30-gauge (0.23-mm diameter) thermocouple wires, and $\dot{q}_{ac}$ is the heat conducted from the balance at ambient temperature to the cell *via* radiation and conduction through the hang-down wire. Numerical estimates indicate $\dot{q}_{bc} \gg \dot{q}_{pc}$. Since heat transferred to the cell is then transferred to the subliming ice (sample), the rate of heat transfer from cell to sample ($\dot{q}_{cs}$) is:

$$\dot{q}_{cs} = \dot{q}_{bc} + \dot{q}_{pc} + \dot{q}_{ac} \qquad \text{(Eq. A18)}$$

The heat transfer rates, $\dot{q}_{ij}$ (i = a, b, c, p; j = c, s, J) are assumed to be of the form:

$$\dot{q}_{ij} = k_{ij}(T_i - T_j) \qquad \text{(Eq. A19)}$$

where k_{ij} are heat transfer parameters and T_i and T_j are the absolute temperatures of apparatus components i and j, respectively. While Eq. A19 is rigorous for heat transfer *via* conduction, the form of Eq. A19 is only an approximation for heat transferred *via* radiation[24].

The probe thermocouple wire makes thermal contact at three points: with the surroundings at ambient temperature (T_a), with the bath at temperature T_b, and with the cell at temperature T_c. The thermal resistance of the wire between the ambient contact and the bath contact is denoted R_{w1}, the thermal resistance of the bath–wire contact (through the apiezon wax) is denoted R_{wb}, and the thermal resistance of the wire from the bath–wire contact to the probe junction is denoted R_{w2}. With these definitions, analysis of the steady-state heat flow in the probe wire yields:

$$\dot{q}_{pc} = k_{pc}(T_p - T_c) = k_{ap}(T_a - T_p) + k_{bp}(T_b - T_p) \qquad \text{(Eq. A20)}$$

where T_p is the probe temperature and k_{ap} and k_{bp} are composite heat transfer coefficients given by:

$$k_{ap} = \frac{R_{wb}}{R_{wb}(R_{w1} + R_{w2}) + R_{w1}R_{w2}} \qquad \text{(Eq. A21)}$$

[24] For radiative heat transfer between two bodies (22):

$$\dot{q}_{ij} = a_{ij}(T_i^4 - T_j^4)$$

where T_i and T_j are the absolute temperatures of bodies i and j, respectively, and a_{ij} depends on system geometry and emissivities of the bodies. When the temperature difference ($T_i - T_j$) is significantly less than the mean temperature ($\overline{T}_{ij}$):

$$\dot{q}_{ij} = 4\,\overline{T}_{ij}^3 a_{ij}(T_i - T_j) = k_{ij}(T_i - T_j)$$

which is of the same form as Eq. A19. However, the k_{ij} parameter for radiative heat transfer is temperature dependent, whereas the corresponding parameter describing conductivity is essentially independent of temperature. As a first approximation, valid for modest temperature ranges, the temperature dependence of k_{ij} for radiative heat transfer can be ignored. Also, for purposes of numerical estimates, the approximation, $a_{ij} = e\sigma A_{ij}$, will be used, where e is the emissivity (1 for the bodies of interest in this research), A_{ij} is the area common to both bodies, and σ is the Stefan-Boltzmann constant.

Table III—Comparison of Microbalance and Vial Resistance Data

l, cm	Normalized Product Resistance ($\hat{R}_p$), cm² hr torr g⁻¹: Vial[a]	Microbalance, Annealed	Microbalance, Quick-Frozen
	5% Potassium Chloride, −21°		
0.27	3.8 ± 0.5[b]	3.0 ± 0.1[b]	7.4 ± 0.5[b]
0.41	4.9 ± 0.6	3.8 ± 0.1	8.4 ± 0.6
0.53	4.9 ± 0.7	4.5 ± 0.2	9.0 ± 0.6
0.70	5.4 ± 0.6	5.4 ± 0.2	9.6 ± 0.7
	5% Povidone, −26°		
0.31	2.4 ± 0.8	2.10 ± 0.05	2.9 ± 0.2
0.48	3.8 ± 0.2	2.65 ± 0.06	3.5 ± 0.3
0.58	4.1 ± 0.1	2.94 ± 0.07	3.9 ± 0.3
0.71	5.0 ± 1.0	3.19 ± 0.08	4.4 ± 0.4
0.92	5.5 ± 0.6	3.79 ± 0.09	5.2 ± 0.4
	System I[c], −21°		
0.17	4.8 ± 0.5		8.5 ± 0.1
0.28	6.0 ± 0.5		10.9 ± 0.1
0.38	7.0 ± 0.4		13.4 ± 0.1
0.48	8.0 ± 0.7		15.9 ± 0.1
	System I[c], −14° (Microbalance), −15° (Vial)		
0.30	6.5 ± 1.8		6.6 ± 0.5
0.48	6.1 ± 1.7		7.1 ± 0.5
0.74	5.8 ± 1.0		7.5 ± 0.6
1.03	6.0 ± 0.8		7.7 ± 0.6

[a] The resistance data represent the mean of four replicate experiments for potassium chloride, two replicate experiments for povidone, and two replicate experiments for System I. [b] Uncertainties are estimated standard errors as calculated from reproducibility of replicate experiments. [c] The microbalance samples are amorphous but the vial samples contain some poorly crystallized mannitol (X-ray and microscopic observations).

and

$$k_{bp} = \frac{R_{w1}}{R_{wb}(R_{w1} + R_{w2}) + R_{w1}R_{w2}} \qquad \text{(Eq. A22)}$$

With perfect thermal contact of the probe wire with the bath ($R_{wb} = 0$), $k_{bp} = R_{w2}^{-1}$, and $k_{ap} = 0$.

Combination of Eqs. A17–A20 and use of the approximations[25] $k_{pc}/k_{bc} \ll 1$, $k_{ac}/k_{bc} \ll 1$, $(T_a - T_i)/(T_a - T_s) = 1$ (i = p, J), yields:

$$T_p - T_s = (1 + r_p\alpha k_{cs}^{-1})(1 + r_p)^{-1}\alpha^{-1}\Delta\overline{H}_s\dot{m} + (1 + r_p)^{-1}[k_{ap}/k_{bp} - k_{aJ}\alpha^{-1}(1 + r_p\alpha k_{cs}^{-1}) - k_{ac}/k_{bc}](T_a - T_s) \qquad \text{(Eq. A23)}$$

$$T_b - T_p = r_p(1 + r_p)^{-1}k_{bc}^{-1}\Delta\overline{H}_s\dot{m} - (1 + r_p)^{-1}(k_{ap}/k_{bp} + k_{aJ}r_pk_{bc}^{-1} + r_pk_{ac}/k_{bc})(T_a - T_s) \qquad \text{(Eq. A24)}$$

and

$$T_b - T_s = \alpha^{-1}\Delta\overline{H}_s\dot{m} - (\alpha^{-1}k_{aJ} + k_{ac}/k_{bc})(T_a - T_s) \qquad \text{(Eq. A25)}$$

with α and r_p defined by:

$$\alpha = k_{bc}k_{cs}(k_{bc} + k_{cs})^{-1} \qquad \text{(Eq. A26)}$$

and

$$r_p = k_{pc}/k_{bp} \qquad \text{(Eq. A27)}$$

The temperature of the subliming ice is denoted T_s.

Since both the bath–cell and probe–cell heat transfer coefficients, k_{bc} and k_{pc}, respectively, include contributions from vapor phase heat conduction, both coefficients are pressure dependent. Using the Smoluchowski theory (12) to relate the thermal conductivity of a gas to pressure, the heat transfer coefficients (k_{ic}, i = p,b) are of the form:

$$k_{ic} = k_{ic}^0\left[1 + \frac{(\bar{a}\Lambda_0/k_r)P}{1 + \bar{a}(\Lambda_0/\lambda)d_iP}\right] \qquad \text{(Eq. A28)}$$

where

$$\bar{a} = \frac{a_c}{2 - a_c}\sqrt{\frac{273.2}{T}} \qquad \text{(Eq. A29)}$$

The energy accommodation coefficient (a_c) is a numerical constant near

[25] As a first approximation, the ratio k_{pc}/k_{bc} is equal to the ratio of the probe area–cell area, which is ~0.06.

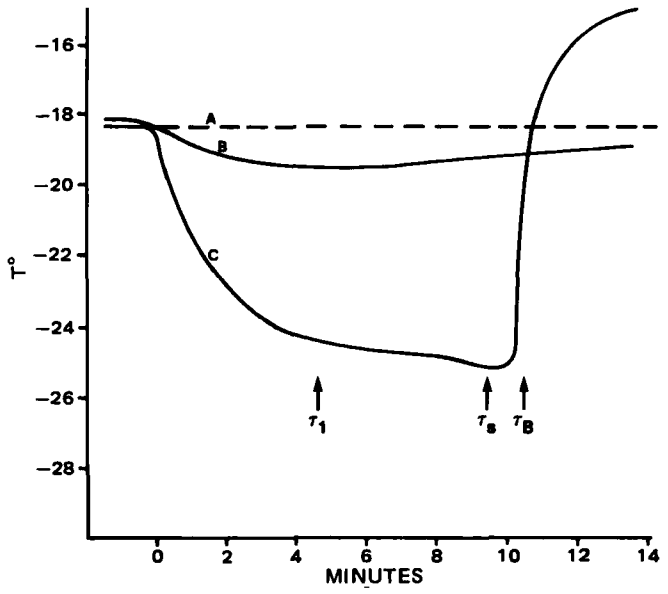

Figure 20—*Temperature* versus *time curve for a calibration experiment at zero pressure using a 10-mg sample of pure water. Key for lines: (A) thermostat; (B) probe; (C) J thermocouple.*

unity (3); k_{ic}^0 represents the radiative heat transfer coefficient; k_r is defined by $k_{ic}^0 = A_i k_r$, where A_i is the area of the probe or cell; Λ_0 is the free-molecule heat conductivity of the gas at 0° (12); λ is the heat conductivity of the gas at ambient pressure (~1 atm); d_i is the separation distance of the hot and cold surfaces, where $d_p = 0.3$ cm and $d_c = 0.6$ cm; P and T are the pressure and absolute temperature, respectively[26].

Preliminary calculations indicate that, as a first approximation, the term $(1 + r_p \alpha k_{cs}^{-1})(1 + r_p)^{-1}$ is essentially independent of pressure. Thus, the pressure dependence in the coefficients of $\dot{m}$ in both Eqs. A23 and A25 is due to the pressure dependence of α, which (from Eqs. A26 and A28) may be written in the form:

$$\alpha^{-1} = (\alpha^0)^{-1} \frac{[1 + (\Lambda_0/\lambda)(d_c + (\lambda/k_r)(1 + k_{cs}/k_{bc}^0)^{-1}P]}{[1 + (\Lambda_0/\lambda)(d_c + \lambda/k_r)P]} \quad \text{(Eq. A30)}$$

where the approximation $\bar{a} = 1$ has been used and the superscript zero on a parameter represents the value of that parameter at zero pressure.

When the sample temperature is not measured directly by a thermocouple embedded in the sample (*i.e.*, as in a normal sublimation experiment), $k_{aJ} = 0$ by definition. A theoretical estimate indicates that k_{ac} is $< 1 \times 10^{-5}$. With this estimate and the experimental value found for k_{bc}, the approximation $k_{ac} = 0$ results in a temperature error of <0.2°. Thus, with $k_{ac} = 0$, combination of Eqs. A23 and A24 gives:

$$T_s = T_p - (1 + r_p^0 \alpha^0 k_{cs}^{-1})(1 + r_p^0)^{-1}\alpha^{-1}\Lambda \bar{H}_s \dot{m} - (1 + r_p)^{-1}(k_{ap}/k_{bp})(T_a - T_p) \quad \text{(Eq. A31)}$$

The parameter k_{cs} in Eq. A31 now refers to the value of the cell–sample heat transfer coefficient in the absence of the J thermocouple wire.

In a temperature calibration experiment the sublimation cell is supported by copper–constantan thermocouple wires (0.23-mm diameter) where the measuring junction (J) is located ~1 mm from the bottom of the capillary tube. This configuration allows the sample temperature to be measured but also prevents the sample mass from being determined. After equilibration of the sample (10.0 mg of pure water) with the thermostat, the chamber was evacuated to the desired pressure and sublimation started. Thermostat, probe, and J thermocouple (T_J) temperatures were monitored as a function of time. When the pressure decreases below ~1 mm and sublimation started (time zero), T_J sharply decreased (Fig. 20) until a steady state was reached at approximately time τ_1. The T_J reading abruptly increased at time τ_B when the ice–vapor interface moved below the bottom of the J thermocouple and thermal contact was broken. When the sublimation rate was high, T_J passed through a minimum at time τ_s, where $\tau_s = 0.9\,\tau_B$. Interpreting τ_s as the time when the ice–vapor interface just covers the measuring junction J, $T_J(\tau_s) = T_s$, where T_s is the temperature of the subliming ice.

In a calibration experiment, the sublimation rate in mg/min at time $\tau_i (i = 1,s)$ is calculated from $\dot{m}_i = (8.8/\tau_B)f_i$, where 8.8 is the difference between the total sample mass of 10.0 mg and the mass remaining at τ_B, the latter calculated assuming the J thermocouple is exactly 1 mm from the bottom of the capillary tube. The factor f_i is the ratio of the sublimation rate at τ_i to the average rate over the time interval $0 \le t \le \tau_B$. This factor, which is near unity, is determined from sublimation experiments where mass is monitored (*i.e.*, no J wire).

A total of 16 calibration experiments were conducted over the bath temperature and chamber pressure ranges $-39° < T_b < -15°$ and $0 < P < 0.6$ mm, respectively, generating the data set (T_b, T_p, T_s, τ_1, τ_s, τ_B, P) for each experiment. These data were used to evaluate the heat transfer parameters appearing in Eqs. A23–A27 *via* regression analysis.

The parameters k_{cs} and k_{aJ} were evaluated by an iterative procedure. First k_{cs} was evaluated from the time dependence of T_J and a preliminary estimate of k_{aJ}, using only data where the sublimation rate was high (Appendix II). Next, k_{bc} and k_{aJ} were evaluated by regression analysis using Eqs. A25 and A30[26]. The resulting value of k_{aJ} was then used to obtain a second approximation of k_{cs}, *etc.* Convergence was obtained after two iterations. Finally, the ratios r_p^0 and k_{ap}/k_{bp} were evaluated from the data by regression analysis using Eqs. A23, A27, and A28. The resulting parameters with their corresponding standard errors are listed in Table IV. Agreement between data and the theoretical model is within the anticipated experimental error. Due to the difficulty in placing the J thermocouple always at the same level in the sample, measurement of the average sublimation rate is subject to sizable random error.

With the evaluated parameters (Table IV), Eq. A31 becomes Eq. 1 (text):

$$T_s = T_p - K_p \frac{(1 + 68.1P)}{(1 + 87.0P)}\dot{m} - K_a(T_a - T_p)$$

where K_p is 10.2 and K_a is 0.010 and 0.006 at $P = 0$ and $P = 0.05$–1.0 torr, respectively. The sublimation rate $\dot{m}$ is in mg/min. In principle, K_a is a smooth function of pressure through r_p. However, the step function representation given above is a simpler yet adequate representation of the data. With the improved probe design described earlier[12], $k_{ap} = 0$ and $r_p \gg 1$ experimentally ($r_p \simeq 14$ in theory). In this case, $K_a = 0$ and $K_p = 7.1$.

Table IV—Values of Heat Transfer Parameters Evaluated from Temperature Calibration Data [a]

Parameter	Value
k_{cs}	$1.55 \times 10^{-3} \pm 0.07 \times 10^{-3}$ cal sec^{-1} °K^{-1}
k_{bc}^0	$2.2 \times 10^{-3} \pm 0.04 \times 10^{-3}$ cal sec^{-1} °K^{-1}
r_p^0	0.61 ± 0.28
k_{ap}/k_{bp}	0.016 ± 0.012

[a] Parameters refer to experiment without a thermocouple embedded in the sample.

APPENDIX II: THEORY OF CELL–SAMPLE HEAT TRANSFER COEFFICIENT

Heat is transferred from the aluminum cell to the sample through the wall and bottom of the glass capillary tube. Since the area available for heat transfer decreases as the length of the ice column decreases during sublimation, the parameter characterizing this heat transfer (k_{cs}) may not be constant. Moreover, in a calibration experiment, the presence of the thermocouple wire in the capillary tube changes the thermal conductivity of the system and, consequently, k_{cs}. The purpose of this section is to present a semiquantitative theoretical argument which indicates that k_{cs} is indeed a constant during sublimation of all but the last traces of ice, and to provide a theoretical basis for the evaluation of k_{cs} under conditions of a sublimation rate experiment (no thermocouple in the sample) using calibration data obtained where a thermocouple is in the sample. The length of the ice column at time zero is denoted L.

A simple steady-state model for heat transfer in the cell–sample system is illustrated by Fig. 21. Heat conducted from ambient to the sample *via* the J thermocouple ($\dot{q}_{aJ}$), assumed to dissipate at the ice–vapor interface, is not shown. The temperature in the aluminum cell (T_c) is assumed independent of the distance variable, x. The ice at the ice–vapor interface ($x = l$) is at a mean temperature T_s, while the average temperature of the

[26] The parameter k_r is calculated from theory (22) with unit emissivity for a temperature of 253°K. For air, literature data (12) for Λ_0 and λ then yield: $\Lambda_0/\lambda = 68.9$ cm^{-1} torr^{-1}, $\lambda/k_r = 0.662$ cm. The distance parameters d_c and d_p are approximately measured as 0.6 and 0.3 cm, respectively. The calculations are not sensitive to small variations in d_c and d_p. The enthalpy of sublimation $\Delta \bar{H}_s$ is 660 cal/g (41).

sample in any volume element of thickness (dx) is T, where T is a function of x.

In any volume element bounded by planes at $x - dx/2$ and $x + dx/2$, the heat flow out of the volume element through the plane at $x - dx/2$ ($\delta\dot{q}_3$) is the sum of the radial heat flow through the container wall ($\delta\dot{q}_1$) and the vertical heat flow into the volume element at the plane $x + dx/2$ ($\delta\dot{q}_2$). The radial heat flow, $\delta\dot{q}_1$, is proportional to the length of the volume element, dx, and the temperature difference $T_c - T$:

$$\delta\dot{q}_1 = k_w dx(T_c - T) \qquad \text{(Eq. A32)}$$

where k_w is a heat transfer coefficient for heat flow through the apiezon wax and the capillary tube wall, and reflects the heat-flow rate for a tube of unit length with a temperature difference of 1° applied. The vertical heat transfer rate is of the form:

$$\delta\dot{q}_i = k_I \frac{(dT)}{(dx)_{x_i}}, \quad i = 2, 3 \qquad \text{(Eq. A33)}$$

where for $i = 2, x_i = x + dx/2$ and for $i = 3, x_i = x - dx/2$. The parameter k_I is the product of the cross-sectional area and the thermal conductivity of the material present in the capillary tube[27]. During a calibration experiment both ice and the J thermocouple wires contribute to k_I. From Eqs. A33 and A32 and the steady-state requirement $\delta\dot{q}_3 = \delta\dot{q}_1 + \delta\dot{q}_2$, we find:

$$\frac{d^2T}{dx^2} = -\frac{k_w}{k_I}(T_c - T) \qquad \text{(Eq. A34)}$$

With the transformation of variables:

$$y = T_c - T \qquad \text{(Eq. A35)}$$

and

$$z = (x - l)/(L - l) \qquad \text{(Eq. A36)}$$

Eq. A34 becomes:

$$\frac{d^2y}{dz^2} - a^2y = 0, \qquad \text{(Eq. A37)}$$

where:

$$a = (L - l)\sqrt{\frac{k_w}{k_I}} \qquad \text{(Eq. A38)}$$

One boundary condition follows from the requirement that the vertical heat flow at the ice–vapor interface ($z = 0$) is equal to the total heat flow from cell to sample ($\dot{q}_{cs}$):

$$\dot{q}_{cs} = -\frac{k_I}{(L - l)}\left(\frac{dy}{dz}\right), \quad z = 0 \qquad \text{(Eq. A39)}$$

where, denoting $\dot{Q}_s$ as the heat removed by sublimation, $\dot{q}_{cs} = \dot{Q}_s - \dot{q}_{aJ}$. This relationship assumes $\dot{q}_{aJ}$ is dissipated at the $z = 0$ surface. $\dot{Q}_s$ is the product of the sublimation rate and the heat of sublimation per gram: $\dot{Q}_s = \dot{m}\Delta\bar{H}_s$. The second boundary condition is obtained from the requirement that $\dot{q}_{cs}$ is given by the sum of the heat flow through the bottom ($\delta\dot{q}_B$) and the integral of $\delta\dot{q}_1$ over the length of the ice column, $0 \leq z \leq 1$. Since $\delta\dot{q}_B = k_B y(1)$, the boundary condition becomes:

$$\dot{q}_{cs} = k_w(L - l)\int_0^1 y(z)dz + k_B y(l), \qquad \text{(Eq. A40)}$$

[27] The parameter k_I is given by:

$$k_I = \pi r^2 \kappa_I$$

where r is the radius of the capillary tube (0.0648 cm) and κ_I is the thermal conductivity of the material within the capillary tube (ice and, in a calibration experiment, the J thermocouple wires of diameter 0.23 mm):

$$\kappa_I = \frac{1}{A_T}\sum_i A_i\kappa_i$$

where, A_T is the total tube cross-sectional area, while A_i and κ_i are the cross-sectional area and thermal conductivity for the ith material (i = ice, copper, constantan).

Based on handbook data for thermal conductivities, k_I (cal cm sec^{-1} °K^{-1}) is calculated as 6.9×10^{-5} for a normal sublimation experiment (without a thermocouple junction in the sample) and 5.0×10^{-4} for a calibration experiment. The parameters k_w and k_B may be estimated from the relationships:

$$k_w = 2\pi r(l_{wx}/\kappa_{wx} + lg/\kappa_g)^{-1},$$

$$k_B = \pi r^2(l_{wx}/\kappa_{wx} + lg/\kappa_g)^{-1}$$

where l_{wx} and κ_{wx} are the thickness and thermal conductivity of the wax, respectively, and l_g and κ_g are the corresponding parameters for the glass tube. By measurement, $l_{wx} = 10^{-2}$ cm, $l_g = 0.037$ cm. Assuming the apiezon wax has the same thermal conductivity as paraffin, $\kappa_{wx} = 6 \times 10^{-4}$ cal cm^{-1} sec^{-1} °K^{-1}. Since $\kappa_g = 2.6 \times 10^{-3}$ cal cm^{-1} sec^{-1} °K^{-1}, $k_w = 1.3 \times 10^{-2}$ cal cm^{-1} sec^{-1} °K^{-1} and $k_B = 4 \times 10^{-4}$ cal sec^{-1} °K^{-1}.

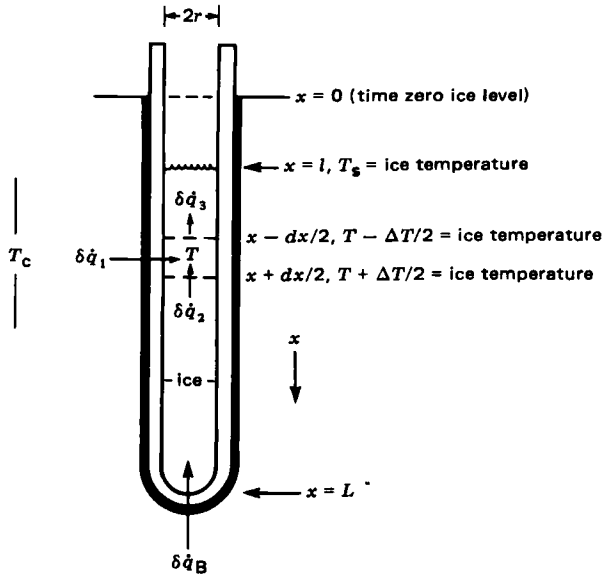

Figure 21—*Schematic of heat flow in the sublimation cell.*

with k_B representing the heat transfer coefficient through the bottom of the capillary tube. Solution of the differential equation (Eq. A37) subject to the boundary conditions (Eqs. A39 and A40) yields:

$$y(z) = b\dot{q}_{cs}\left\{e^{-az} + \frac{e^{-a}(1 - bk_B)\cosh(az)}{\cosh(a)[\tanh(a) + bk_B]}\right\} \qquad \text{(Eq. A41)}$$

where:

$$b^{-1} = \sqrt{k_w k_I} \qquad \text{(Eq. A42)}$$

The constant k_{cs}, defined by $\dot{q}_{cs} = k_{cs}(T_c - T_s)$ where $(T_c - T_s) = y(z = 0)$, is then:

$$k_{cs} = b^{-1}\frac{[\tanh(a) + bk_B]}{[1 + bk_B\tanh(a)]} \qquad \text{(Eq. A43)}$$

The parameter k_I (cal cm sec^{-1} °K^{-1}) is 6.9×10^{-5} with only ice in the capillary tube and is 5.0×10^{-4} in a calibration experiment where thermocouple wires are present[27]. Rough estimates[27] yield, $k_w = 1.3 \times 10^{-2}$ cal cm^{-1} sec^{-1} °K^{-1} and $k_B = 4 \times 10^{-4}$ cal sec^{-1} °K^{-1}. Therefore, in a sublimation rate experiment (no J wire) $\sqrt{k_w/k_I} = 14$ and for $L - l > 0.1$ cm (through ~90% of the sublimation experiment), $a > 1.4$ and Eqs. A41 and A43 simplify to give:

$$y(z) = b\dot{Q}_s e^{-az}, \quad L - l > 0.1 \text{ cm} \qquad \text{(Eq. A44)}$$

and

$$k_{cs} = \sqrt{k_w k_I}, \quad L - l > 0.1 \text{ cm} \qquad \text{(Eq. A45)}$$

As the last traces of ice are sublimed, $l \approx L$ and $k_{cs} = k_B$. Since the estimates indicate $k_B \ll \sqrt{k_w k_I}$, the theory suggests that as $l \to L$, the value of k_{cs} should decrease sharply causing a decrease in ice temperature and a corresponding decrease in the sublimation rate in those cases where the sublimation rate is high. This qualitative prediction is verified in experiments with pure water at high temperature (*i.e.*, −20°) where the sublimation rate is found to sharply decrease when $L - l$ is ~0.1 or less.

Equation A41 may be used to evaluate k_w from the time dependence of T_J determined in a calibration experiment. The resulting value of k_w may then be used with the calculated value of k_I to evaluate k_{cs} using Eq. A43. Denoting T_J as the temperature measured by the thermocouple junction in the sample at location x_J, $T_c - T_J = y(z_J)$, where z_J is given by Eq. A36 with $x = x_J = 0.72$ cm[28]. Equation A41 and the relationship $T_b - T_c = k_{bc}^{-1}\dot{q}_{cs}$ then results in:

$$\left(\frac{T_b - T_J}{\dot{q}_{cs}}\right) = k_{bc}^{-1} + b \cdot G(k_w, l) \qquad \text{(Eq. A46)}$$

where the function $G(k_w, l)$ denotes the terms enclosed in brackets on

[28] At time τ_s, the J thermocouple measures the surface temperature of the ice, the surface located at x_J. From the interpretation given earlier, x_J represents the value of x at the top of the thermocouple measuring junction. Since the junction head is ~0.5 mm in diameter and the bottom of the junction is at $x = 0.77$ cm, $x_J = 0.72$ cm. Since $l = x_J$ at time τ_s and $L = 0.87$ cm, $L - l = 0.15$ cm at τ_s.

the right-hand side of Eq. A41. As indicated, G depends on k_w and the position of the ice–vapor interface, which in turn depends on time. The time when the ice–vapor interface is at the same location as the thermocouple (*i.e.*, $az_J = 0$) is denoted τ_s. The time τ_1 represents a time large enough to establish steady-state heat flow but small enough so that the ice–vapor interface is still several millimeters above the thermocouple. With the above definitions for τ_s and τ_1:

$$\left(\frac{T_b - T_J}{\dot{q}_{cs}}\right)_{\tau_s} - \left(\frac{T_b - T_J}{\dot{q}_{cs}}\right)_{\tau_1} = H(k_w) \qquad \text{(Eq. A47)}$$

where for fixed τ_s and τ_1, H is a function of k_w only, given by:

$$H(k_w) = (k_w k_I)^{-1/2}\left\{\exp(-a_1 z_1) + \frac{\exp(-a_s)(1 - bk_B)}{\cosh(a_s)[\tanh(a_s) + bk_B]} - \frac{\exp(-a_1)(1 - bk_B)\cosh(a_1 z_1)}{\cosh(a_1)[\tanh(a_1) + bk_B]}\right\} \qquad \text{(Eq. A48)}$$

where a_s and a_1 are values of the parameter a (Eq. A38) at times τ_s and τ_1, respectively, and z_1 is the value of z_J (Eq. A36 with $x = x_J$) corresponding to time τ_1. Equation A48 is not sensitive to the precise choice of τ_1. For convenience, τ_1 is always taken as $\tau_1 = 0.4\,\tau_B$, where τ_B is the time for the ice–vapor interface to move below the bottom of the J thermocouple. Sublimation rate experiments (no J wire) indicate that with a sample of 10.0 mg of water ($L = 0.87$ cm), $L - l = 0.53$ cm at τ_1 (= $0.4\tau_B$). Thus, from Eq. A36, $z_1 = 0.72$[28]. The parameter k_B is related to k_w by $k_B = (r/2)k_w$[27] with r representing the radius of the capillary tube (0.0648 cm.). Since k_I may be calculated from theory[27], a_1, a_s, and k_B depend only on k_w and $H(k_w)$ is easily tabulated as a function of k_w.

With $\dot{q}_{cs} = \dot{Q}_s - k_{aJ}(T_a - T_J)$, and $\dot{Q}_s = \Delta\overline{H}_s\dot{m}$, values of $\dot{q}_{cs}$ at times τ_1 and τ_s are evaluated from the sublimation rates ($\dot{m}$) at these times and a value of k_{aJ} is estimated from the calibration data. Sublimation rates are evaluated from τ_B data as outlined in Appendix I. Using only data where the sublimation rate is high, the value of k_{cs} is relatively insensitive to the choice of k_{aJ}.

Thus, with T_b, T_J, and $\dot{q}_{cs}$ determined at τ_s and τ_1, $H(k_w)$ is determined from the data, which then determines an experimental value for k_w. The iterative procedure outlined in Appendix I determines both k_{aJ} and k_w, yielding the result $k_w = 0.035 \pm 0.003$. For a sublimation rate experiment (no J wire), $k_I = 6.9 \times 10^{-5}$ cal cm sec^{-1} °K^{-1} [27], which then gives (Eq. A45) $k_{cs} = 1.55 \times 10^{-3}$ cal sec^{-1} °K^{-1}. The value of k_w obtained is larger than the theoretically estimated value[27]. A strict interpretation of the theory would imply that the wax sealing the capillary tube in the aluminum cell offers essentially zero thermal resistance. However, the difference between the experimental and theoretical k_w values probably reflects, in large part, the theory's neglect of vertical heat transfer in the walls of the glass capillary tube. In any case, use of the experimental k_w should yield a reliable value of k_{cs} for experimental use.

REFERENCES

(1) B. J. Luyet, *Ann. N.Y. Acad. Sci.*, **125,** 502 (1965).

(2) A. P. MacKenzie, *Transplant. Proc.*, 8 (Suppl. 1), 181 (1976).

(3) A. P. MacKenzie, *Bull. Parenter. Drug Assoc.*, **20,** 101 (1966).

(4) M. J. Pikal, A. L. Lukes, and J. E. Lang, *J. Pharm. Sci.*, **66,** 1312 (1977).

(5) K. Ito, *Chem. Pharm. Bull.*, **18,** 1509 (1970).

(6) K. Ito, *Chem. Pharm. Bull.*, **18,** 1519 (1970).

(7) K. Ito, *Chem. Pharm. Bull.*, **19,** 1095 (1971).

(8) R. Patel and A. Hurwitz, *J. Pharm. Sci.*, **61,** 1806 (1972).

(9) S. L. Nail, *J. Parenter. Drug Assoc.*, **34,** 358 (1980).

(10) D. Saravacus, *Food Technol.*, **19,** 193 (1965).

(11) J. D. Mellor, "Fundamentals of Freeze-Drying," Academic, New York, N.Y., 1978.

(12) S. Dushman and J. M. Lafferty, "Scientific Foundations of Vacuum Technique," 2nd. ed., Wiley, New York, 1962.

(13) A. P. MacKenzie, *Ann. N.Y. Acad. Sci.*, **125,** 522 (1965).

(14) H. Seager, *Manuf. Chem. Aerosol News*, **Feb.,** 41 (1979).

(15) L. F. Ginette, R. P. Graham, and A. I. Morgan, Jr., *Trans. 5th. Natl. Vac. Symp.*, 268 (1958).

(16) G. D. Saravacos, *Food Technol.*, **19,** 193 (1965).

(17) T. Nei, H. Souzu, and N. Hanafusa, *Low Temp. Sci., Ser. B*, **21,** 71 (1963).

(18) J. L. Stephenson, *Bull. Math. Biophys.*, **15,** 411 (1953).

(19) A. P. MacKenzie and B. J. Luyet, *Biodynamica*, **9,** 193 (1964).

(20) J. Flink and F. Geyl-Hansen, *Rev. Sci. Instrum.*, **49,** 269 (1978).

(21) J. R. Partington, "An Advanced Treatise on Physical Chemistry," Vol. 1, Wiley, New York, N.Y., 1949.

(22) J. H. Perry, "Chemical Engineer's Handbook," 4th ed., McGraw-Hill, New York, N.Y., 1963.

(23) J. Amoignon, "Freeze-Drying and Advanced Food Technology," Academic, London, 1975, p. 445.

(24) "International Critical Tables," vol. 4, McGraw-Hill, New York, N.Y., 1978, p. 259.

(25) R. Toei, M. Okazaki, and M. Asaeda, *J. Chem. Eng.*, 8, 277 (1977).

(26) K. Tschudin, *Helv. Phys. Acta*, **19,** 91 (1946).

(27) J. G. Davy, Ph.D. Dissertation, Univ. of California, Berkeley, 1970.

(28) N. F. Ho and T. J. Roseman, *J. Pharm. Sci.*, **68,** 1170 (1979).

(29) B. Couriel, *Bull. Parenter. Drug Assoc.*, **31,** 227 (1977).

(30) R. M. Barrer, *Appl. Mater. Res.*, **2,** 129 (1963).

(31) F. O. Goodman and H. Y. Wachman, "Dynamics of Gas-Surface Scattering," Academic, New York, N.Y. 1976.

(32) E. A. Flood, R. H. Tomlinson, and A. E. Leger, *Can. J. Chem.*, **30,** 348 (1952).

(33) A. W. Adamson, "Physical Chemistry of Surfaces," Interscience, New York, N.Y., 1960.

(34) M. Kaiho, M. Chikazawa, and T. Kanazawa, *Nippon Kagaku Kaishi*, **1972,** 1386.

(35) H. Walter, *Z. Phys. Chem. (Frankfurt/Main)*, **75,** 287 (1971).

(36) T. Kanazawa, M. Chikazawa, M. Kaiho, and T. Fujimaki, *Nippon Kagaku Kaishi*, **1973,** 1669.

(37) J. R. Dacey, "Solid Surfaces and the Gas-Solid Interface," Advances in Chemistry Series, No. 33, American Chemical Society, Washington, D.C., 1961.

(38) J. R. Dacey, *Ind. Eng. Chem.*, **57,** 27 (1965).

(39) E. A. Flood, R. H. Tomlinson, and A. E. Leger, *Can. J. Chem.*, **30,** 389 (1952).

(40) O. Knacke and D. Neuschutz, *Z. Phys. Chem. (N.F.)* **71,** 247 (1970).

(41) G. Janesco, J. Pupezin, and W. A. Van Hook, *J. Phys. Chem.*, **74,** 2984 (1970).